D12.3 – CCT2 Synthesis report on predicted impacts & uncertainties

Introduction

The initial concept for this synthesis report was to follow a number of explicit leakage scenarios from the reservoir, assessing flow rates and environmental impact and ending with an economic analysis. However because at each stage of the trail the number of variables, scenarios and uncertainties multiply, this approach was replaced by a more pragmatic approach which addressed the primary scenario space at each stage. For example for any given reservoir leakage scenario there are multiple possible flow pathways through the overburden, a range of trapping and buffering possibilities within the overburden, multiple possibilities of CO_2 bubble plume size and resultant water column plume dynamics, a wide range of hydrodynamic conditions which fundamentally change the size and shape of chemical perturbation in the natural environment and many different biological communities that may be impacted. On top of this a cost analysis must cope with a wide range of economic scenarios involving national and global responses (or the lack of) to climate change, energy generation and emissions reduction. Consequently, we initiated the exercise by identifying a small range of geologically plausible reservoir leakage scenarios, associated with Sleipner and Snøhvit, so that the following analysis was at least grounded in realism, rather than speculation. Hence 4 representative scenarios (table 1) were simulated addressing different potential leakage structures documented in the larger Sleipner and Snøhvit areas (see section 1.1).Whilst the leakage pathway modelling within the overburden and water column has taken the approach of using these specific scenarios (sections 1 & 2), the impact and economic analysis (sections 4 & 5) has taken a generic approach with the economic analysis taking a top-down approach.

Scenario	max CO_2 leakage at seafloor	Footprint at seafloor
Seismic Chimney	150 T/d	500 m diameter
Fault / Fracture	15 T/d	200 x 2000 m^2 fracture
Blowout	150 T/d	50 m diameter
Well / borehole	20 T/yr (= 0.055 T/d)	Few meters diameter

Table 1. Representative scenarios used to inform impact analysis.

The two scenarios for leakage through a seismic chimney and a geological fault are based on typical geological structures known to act as fluid flow pathways (e.g., Andresen, 2012; Berndt, 2005; Gay et al., 2012; Judd and Hovland, 2007). The maximum CO_2 leakage through these structures was derived numerically (see section 1.2). The blowout and the well scenarios were derived from observed

hydrocarbon leakage at the North Sea blowout site well 22/4b (Leifer and Judd, submitted) and abandoned wells in the Sleipner area (Vielstädte et al., revised).

1. Leakage through sedimentary overburden

1.1 Leakage Pathways

In addition to man-made boreholes, several geological structures acting as pathways for leakage of CO_2 have been identified in the study areas around Sleipner and Snøhvit. These have been classified into 3 types: (a) permeable faults, (b) seismic chimneys, and (c) seismic pipes.

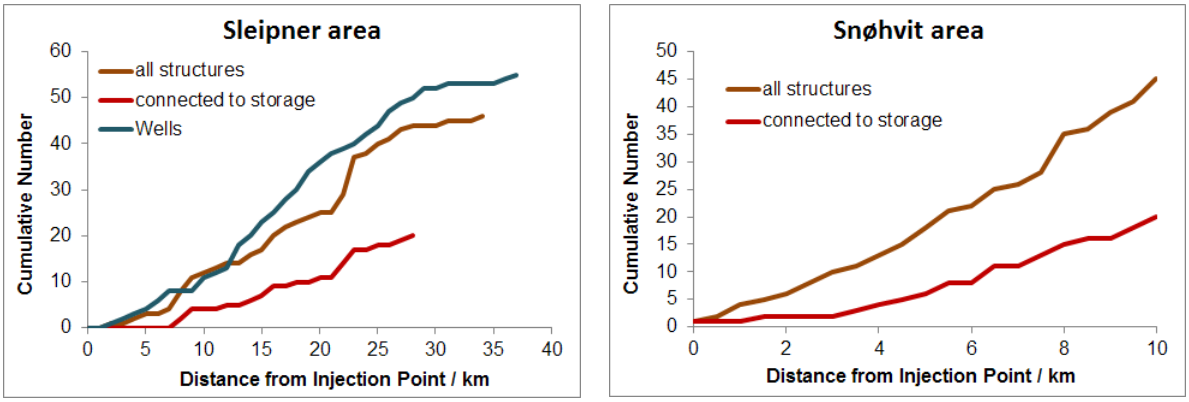

Figure 1: Total number of potential leakage structures and those connected to the CO_2 storage unit in the Sleipner (left) and the Snøhvit (right) areas.

Overall, 40-50 % of the identified structures in both areas are connected to the respective CO_2 storage unit and, thus, pose a relevant risk for leakage should the CO_2 plume reach these structures. Plotting the total number of leakage structures and those with connection to the storage unit illustrates this measure (Fig. 1).

1.1.1 Leakage structures at Sleipner

The Sleipner area hosts a multitude of manifestations for fluid flow, including gas pockets, sediment mobilizations, seismic pipes and chimneys, in the overburden of the Utsira formation (Fig. 2). In our analysis, we applied the terminology of Andresen (2012), who defined ‘seismic pipes’ as narrow, strictly columnar seismic anomalies associated with stacks of high amplitudes and ‘seismic chimneys’ as dimmed or distorted seismic amplitude anomalies of complex shape and much larger dimensions. In total, 44 seismic chimney structures have been identified in the shallow overburden of the Utsira formation, i.e. above the Top Pliocene horizon, because only these structures may constitute conduits to the sediment surface. Based on their seismic appearance, the structures can be subdivided into three

categories, A, B and C (Fig. 2). The difference in the seismic appearance most likely results from different geological properties and formation characteristics.

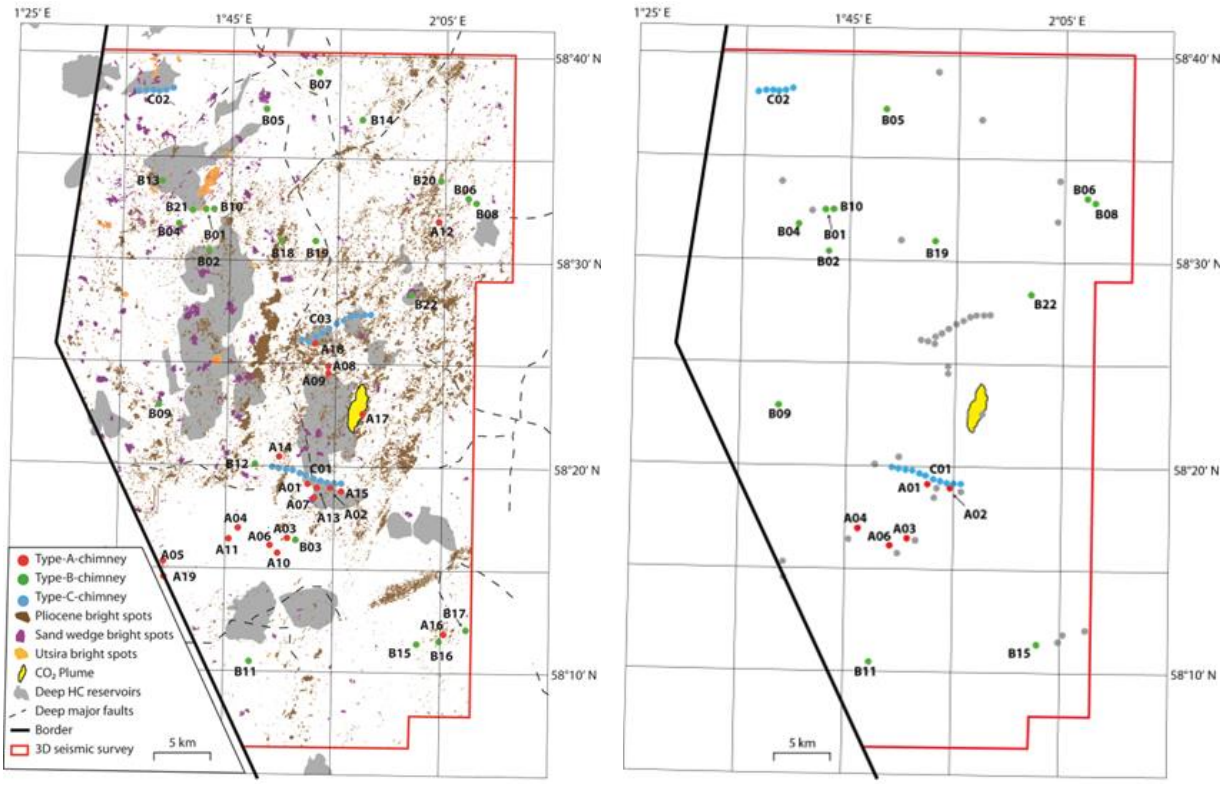

Figure 2: Maps of (left) fluid flow manifestations in the overburden of the investigated area around Sleipner (Karstens and Berndt, revised) and (right) chimney structures with (red, green, blue dots) and without (gray dots) connection to the Utsira Formation.

The seismic interpretation revealed different source depths for the chimneys, most of them originating in the Upper Pliocene horizon or the Utsira Formation. Chimneys terminating well above the Utsira Formation (e.g. at the Top Pliocene horizon) are disregarded as potential leakage pathways (grey coloured structures in Fig. 2, right). Thus, only 19 of a total of 44 chimney structures in the investigated area show evidence for a connection to the Utsira Formation. However, many of these structures are located at significant distance from the CO_2 injection point and the current outline of the CO_2 plume (yellow colour in Fig. 2). Assuming a continuation of the plume migration mainly in N-S direction, chimney structures A01, A02, B19, B22, and C01 (see Appendix 1 for detailed information) appear most relevant for a risk assessment. Type-C chimneys are currently re-evaluated in terms of seismic interpretation because they are possibly caused by imaging artefacts.

1.1.2 Leakage structures at Snøhvit

At Snøhvit a much smaller area around the CO_2 injection site has been investigated. A total number of 45 potential leakage structures, including wells, faults, and seismic chimneys (Fig. 3), were identified in the sedimentary overburden within a distance of 10 km around the injection point. Linjordet and Olsen (1992) classify several faults in the NW of the study area as impermeable for fluid flow. Overall 20 of the identified structures that connect directly to the storage unit are considered as permeable and hence, pose an immediate risk for leakage.

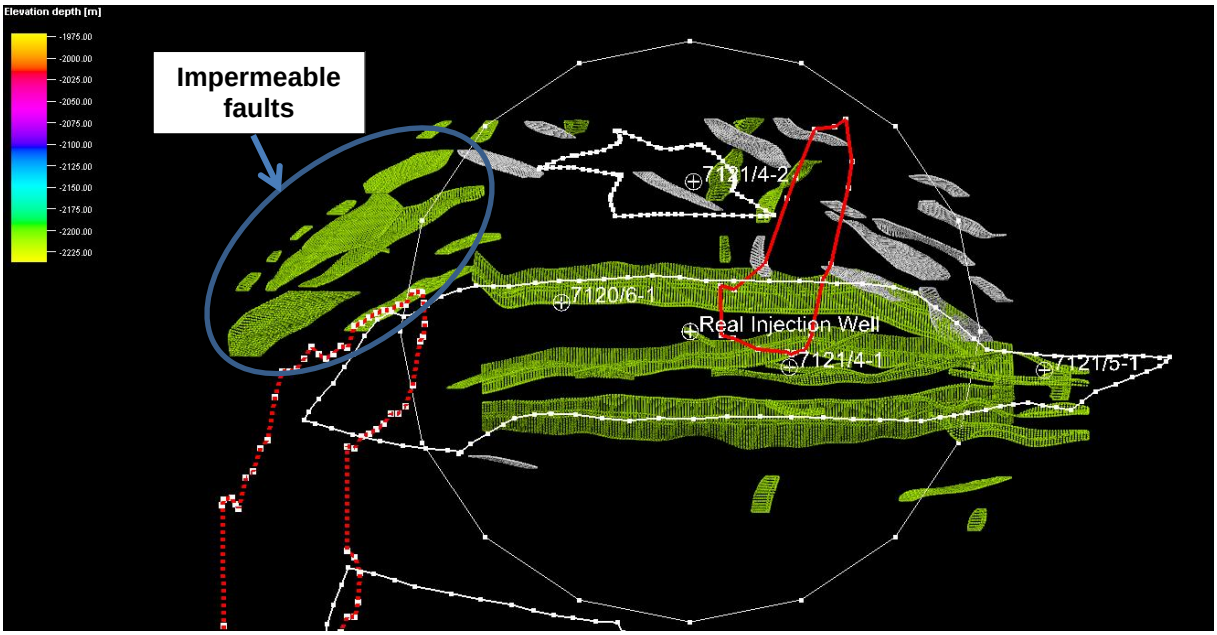

Figure 3: Map of geological structures identified in the area around Snøhvit.

1.2 Leakage rates through overburden and impacted area at seafloor

1.2.1 Sleipner simulations

For the Sleipner area a full 3-D hydrogeological model including the Utsira Formation, the complete sedimentary overburden up to the seafloor and the identified leakage structures was set up. The numerical simulations were fine-tuned to match the CO_2 plume outlines determined by 4-D time-lapse seismic surveys since the start of the injection in 1996 (e.g., Arts et al., 2008; Chadwick et al., 2009). The best match was achieved by introducing a laterally anisotropic permeability distribution in the Utsira Formation ($K_y/K_x = 10$; Tab. A2.1 in Appendix 2). Simulations suggest CO_2 dissolution will become important after about 30 years.

Numerical simulations predict that the CO_2 will reach the nearest leakage structures, seismic chimneys A02 and C01 (Fig. 2), and start to leak into the North Sea after ~150 years of continuous injection (Fig. 4). The leakage rate into the water column will further increase up to a maximum of ~110 t/d until the injection is stopped (after 200 years in the depicted simulation). Upon injection stop the leakage rate will drop quickly by a factor of 10 and then tail out slowly over many centuries (Fig. 4). The

resulting footprint of the CO_2 leak at the seafloor is ~0.1 km^2 (see Appendix 2 for more information).

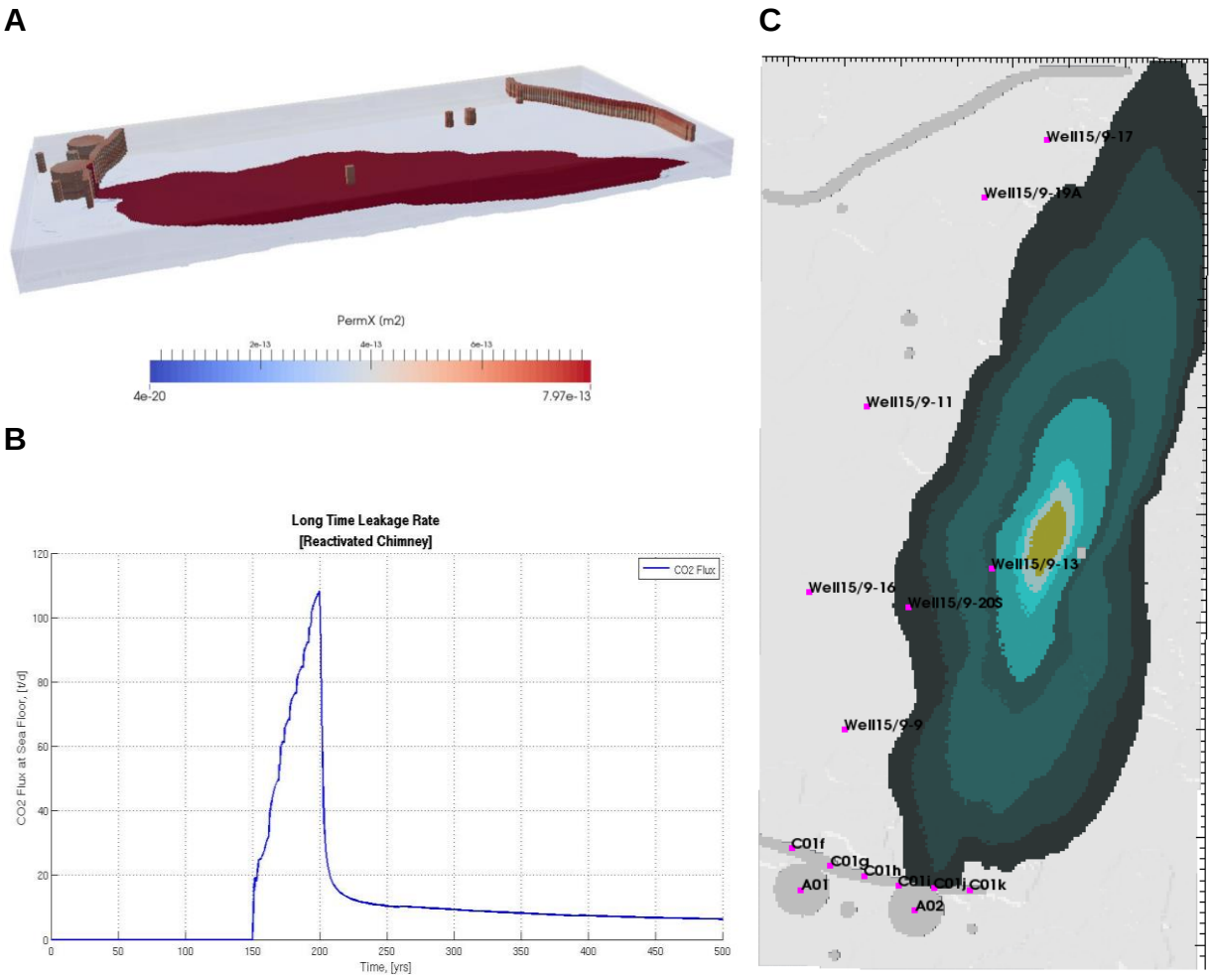

Figure 4: Simulations of the temporal spread, migration and leakage of the CO_2 injected into the Utsira Formation. (A) Model domain with permeability distribution in the leakage structures showing the extent of the CO_2 plume after 160 years of continuous injection (rate of 1 Mt/yr). (B) Predicted CO_2 leakage through seismic chimney A02 at the seafloor within the first 500 years; CO_2 injection is stopped after 200 years. (C) Outline of the CO_2 plume in the storage unit 6, 9, 13, 30, 50, 100, 150, and 200 years after the start of the injection.

1.2.2 Snøhvit simulations

The simulated scenarios at Snøhvit consider the injection of 0.7 Mt/yr of CO_2 over 20 years. The predicted profiles of leakage through the 3 simulated leakage structures, Seismic Chimney, Fault/Fracture, and Blowout, have a characteristic shape over time for all scenarios (Fig. 5), with a maximum leakage flow occurring directly after the initial break-through at the seafloor followed by a trailing decrease over several decades to hundreds of years (depending on the maximum flow occurring). The final

resulting low flow continues for thousands of years (maximum simulation time was 2000 years). The time for CO_2 break-through at the sediment surface, the maximum leakage flow and the decay time primarily depend on the factors: (i) permeability of the background and leakage structure, (ii) size of the leakage structure, (iii) distance between the injection spot / CO_2 plume and the leakage structure.

Very large structures, such as faults and seismic chimneys, are eventually only partially percolated by the leaking CO_2, so that our numerical simulations do not predict maximum leakage flows larger than 150 t/d. If the distance between injection spot and leakage structure is ~1 km, our simulations estimate leakage at the seafloor in the Snøhvit area to occur 30-50 years after start of the injection and the affected area of seafloor to be at maximum ~0.2 km^2 (Fig. 5).

1.2.3 Leakage through abandoned wells

Smaller leakage structures will reduce the maximum leakage flow by 1-2 orders of magnitude and consequently also affect a much smaller area of seafloor. For example, using a semi-analytical model Nordbotten et al. (2005) calculate leakage fluxes through abandoned wells to be 10^3-10^4 times smaller than the corresponding CO_2 injection rate. Even lower leakage fluxes, i.e. ~20 t/yr with a footprint of a few metres in diameter, were observed for methane ebullition at abandoned wells in the Sleipner area (Vielstädte et al., revised). Here, gas buoyancy is likely the primary driver for the leakage. We have chosen this latter situation for our low-flux leakage scenario 'Well/Borehole' (Fig. 5).

1.2.4 Geomechanical effects

Geomechanical effects associated with CO_2 injection may pose an additional uncertainty factor in estimating leakage rates (e.g. Zoback and Gorelick, 2012). The flow through faults and fractures is usually stress-dependent, which implies that pressure build-up associated with CO_2 injection causes fault dilation (i.e. an increase in fault aperture), which in turn makes faults more conductive. Fault transmissivity can increase several times, even by a few orders of magnitudes, as the transmissivity through a fault is proportional to cube of aperture (cubic law). Besides dilation, pressure build-up can also cause shear slip on the fault (i.e. fault re-activation), which can also lead to an increase in fault conductivity. Ongoing numerical simulations of the partner TNO aim to provide additional insights into the impact of geomechanical stress changes on hydro-mechanical behaviour of faults.

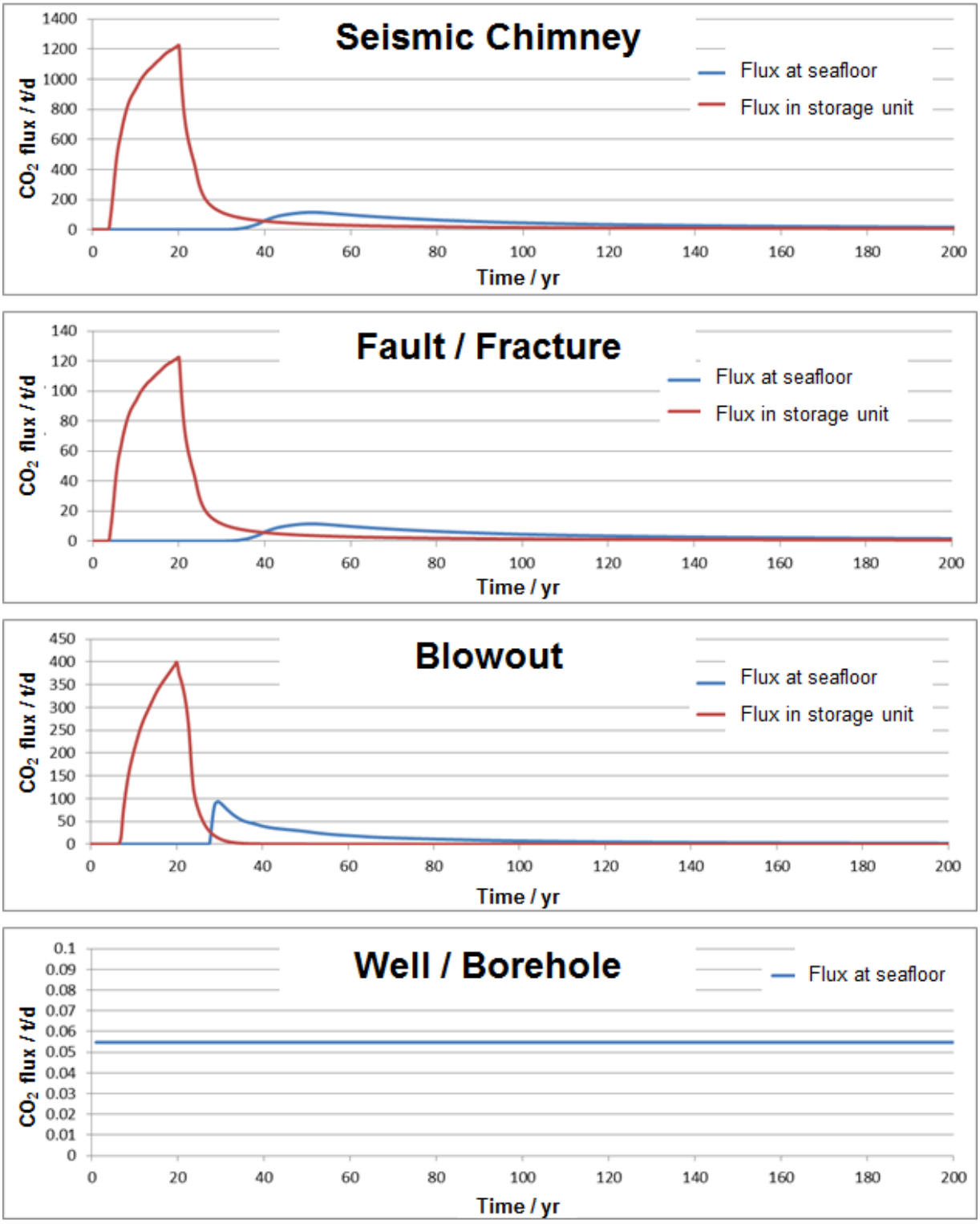

Figure 5: Simulated CO_2 leakage rates at the seafloor (blue) and at the base of the leakage structures at reservoir depth (red) for the 3 scenarios 'Reactivated chimney', 'Fault/Fracture', and 'Blowout'. The constant flux for the 'Well/Borehole' scenario was derived from observed methane leakage at abandoned wells in the Sleipner area (Vielstädte et al., revised).

1.3 Impact on sediment geochemistry

During its ascent to the seafloor, the gaseous or liquid CO_2 will dissolve in the porewater of the leakage structure, lowering the local pH and induce dissolution of $CaCO_3$ and reactive silicate minerals. The mineral dissolution is the ultimate sink of CO_2 as it converts the CO_2 into HCO_3^-, thereby buffering the pH of the porewater. The corresponding reaction rates can be ordered as follows: CO_2 dissolution >> $CaCO_3$ dissolution > silicate dissolution.

A

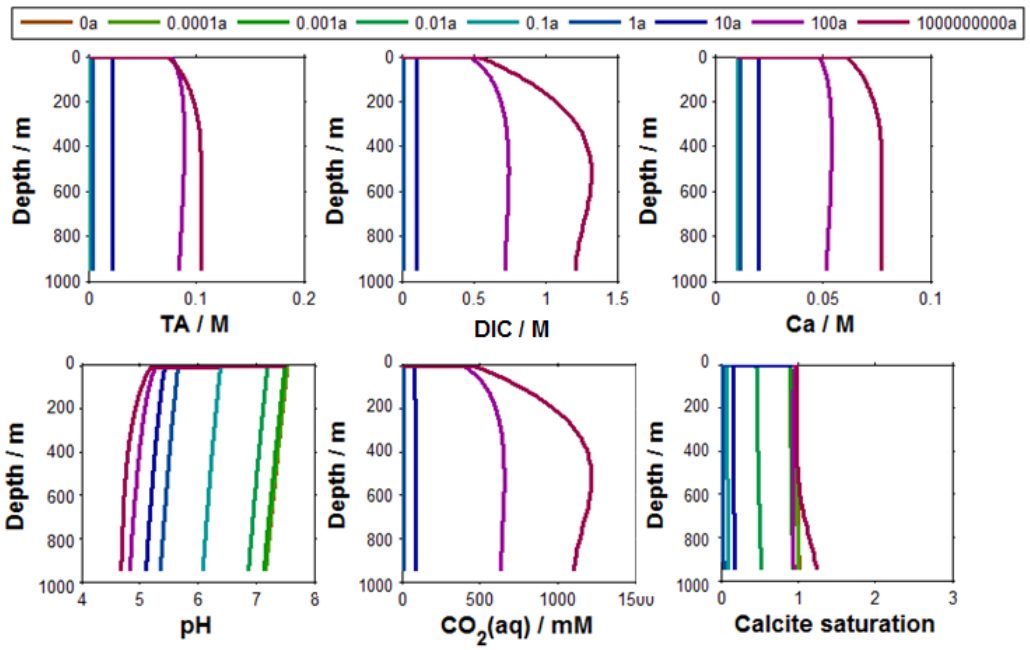

B

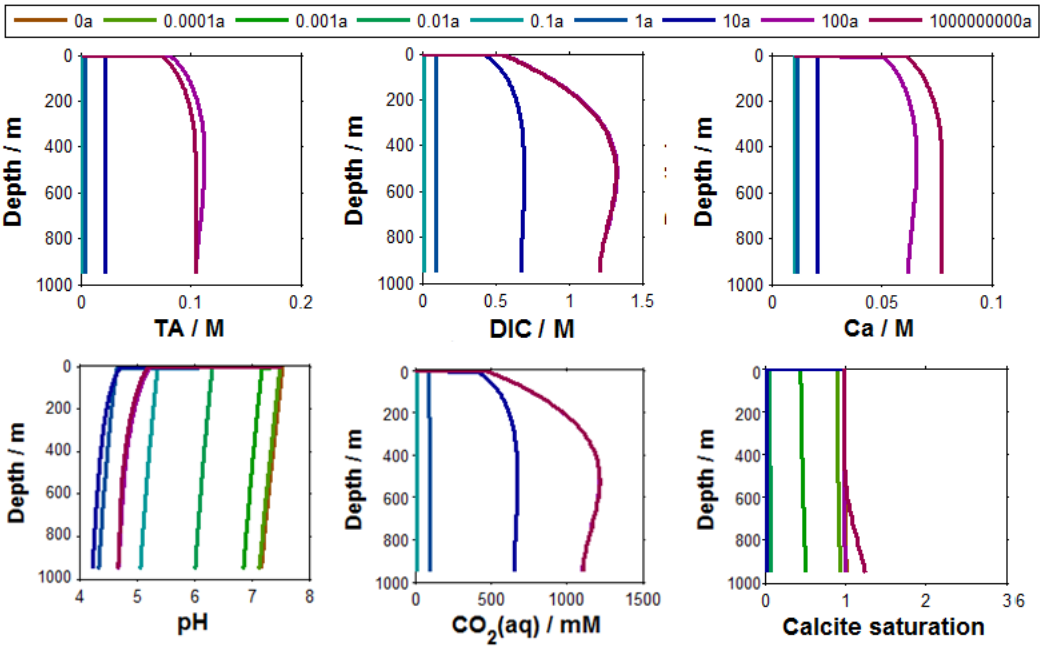

C

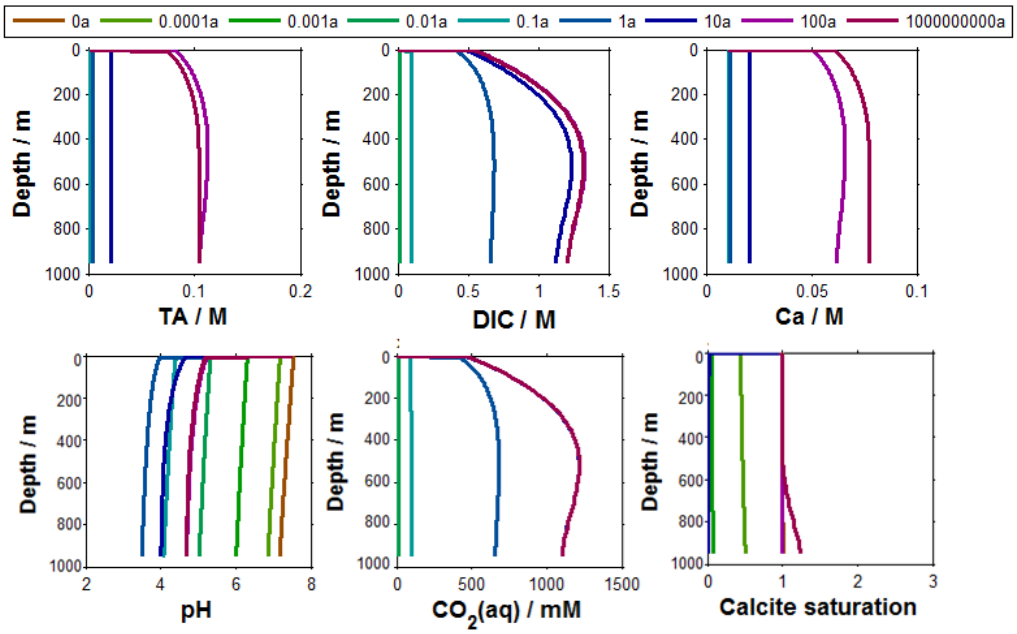

Figure 6: Simulated temporal evolution of porewater concentrations of total alkalinity (TA), dissolved inorganic carbon (DIC), dissolved Ca, pH, dissolved CO_2, and calcite ($CaCO_3$) saturation in the leakage pathway for different rate constants of CO_2 dissolution: (A) 10 mM/yr; (B) 100 mM/yr; (C) 1000 mM/yr. Information on the model setup is provided in Appendix 2.

Dissolution of CO_2 into the porewater will proceed until the porewater is saturated with respect to CO_2 (compare Figs. 6 and A2.5). Depending on the respective rate this may initially lower the pH below 4. Buffering from calcium carbonate dissolution will then kick in and raise the pH until equilibrium with respect to $CaCO_3$ is reached. At Sleipner the buffer pH is 4.7-5 producing a total alkalinity of ~0.11 M (Fig. 6). In the absence of significant porewater advection, this situation may even be reached before all the carbonate minerals in the sediment are dissolved. As a consequence, the gaseous CO_2 phase will then fully break through. From our simulations it can be estimated that dissolution of CO_2 and subsequent weathering reactions in the leakage pathway may postpone the breakthrough time of the CO_2 gas by a few years to decades, primarily depending on the leakage flux, the CO_2 dissolution rate, and the amount of reactive minerals present in the sediment.

Another reaction that has the potential to even completely seal a CO_2 leak is the formation of CO_2 hydrate. This possibility is given, when a storage site in water depths larger than ~250 m, such as is the case in Snøhvit, is chosen. In the event of leakage the CO_2 will enter a zone in the shallow overburden, where temperatures become low enough (i.e. <10 °C) for CO_2 hydrate formation to occur. The CO_2 hydrates will fill the pore space and throats, thereby reducing the permeability in the leakage structure by many orders of magnitude until further CO_2 ascent comes to a halt. In laboratory experiments within work package 2 we have quantified the permeability reduction, k/k_0, as a function of hydrate saturation, S_H: $k / k_0 = (1 – S_H)^n$ with $n \approx 12$ (Kossel et al., 2014; see D2.4 for experimental and modelling details).

2. Leakage into water column

In the water column, the CO_2 gas bubbles will generally dissolve within 5 m above the seafloor (depending on the bubble size) and the dissolved, low-pH plume will disperse quickly due to currents and tides.

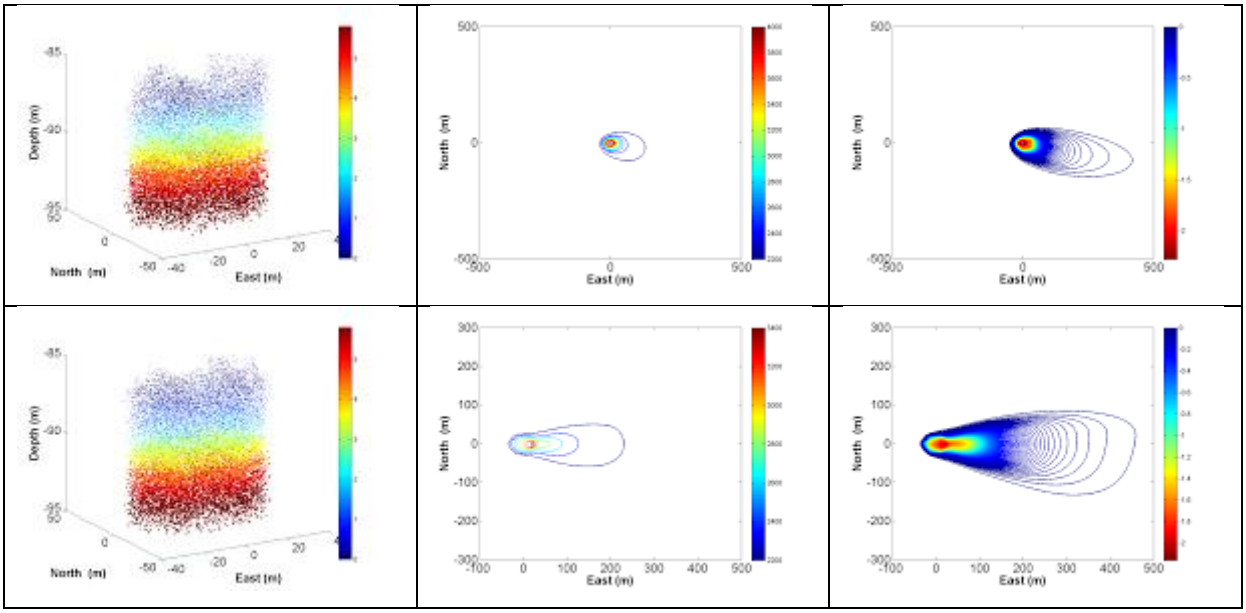

Figure 7: Simulation of gas bubble dissolution in the water column (left column) for the Blowout scenario (150 T/d emitted over a circular area of 50 m in diameter) and resulting maximum DIC (middle column) and pH change (right column) distribution for 2 different current strengths (top: 9 cm/s; bottom: 20 cm/s).

For the Blowout scenario (150 T/d over 50 m diameter at seafloor), the footprint of the dissolved CO_2 plume in the water column is strongly dependent on the prevailing current and may extend by a few hundreds of metres (Fig. 7).

A similar distribution pattern is also predicted using a full 3-D ocean circulation model (BOM) considering the North Sea current and tidal forcing at Sleipner (Fig. 8). The resulting CO_2 concentrations are much lower (at maximum ~50 µM), because the model grid sizes are larger (800 x 800 x 5 m^3) than the maximum extent of the CO_2 plume (Fig. 7).

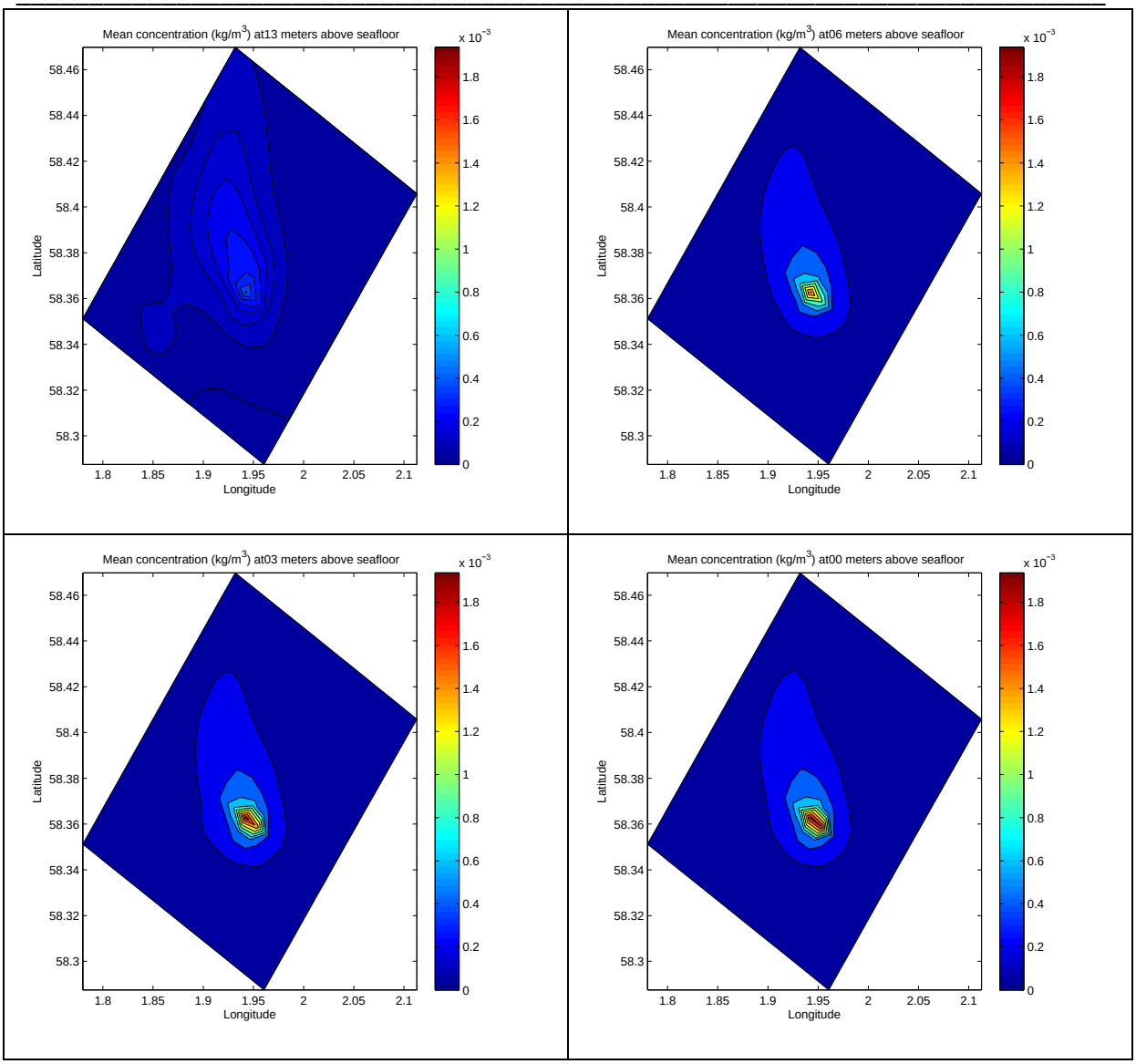

Figure 8: Spatial extent of the dissolved CO_2 plume predicted by the BOM for the Blowout / Chimney scenario at the Sleipner area.

Simulations of the leaky well scenario (20 T/a) show similar results with a very narrow plume extending up to 35 m in current direction (Fig. 9). The change in pH is highest at low current velocities (-0.55 pH units at 0.1 m/s) and lowest at high current velocities (-0.25 pH units at 0.25 m/s).

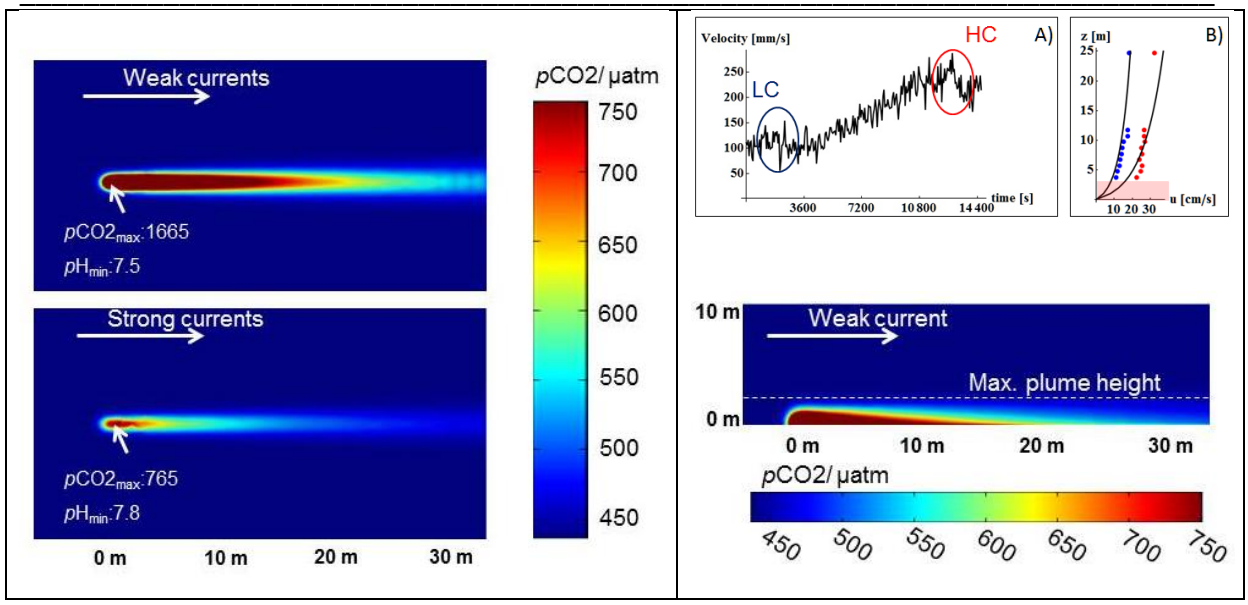

Figure 9: Simulation of the leaking well scenario at low and high current velocities. (left) Contour plot of pCO_2 footprint at the seafloor. (right top) North Sea current velocities measured at Sleipner used for the simulation (right bottom). Contour plot of the pCO_2 distribution above the seafloor in current direction.

Even though the models used for simulating the dissolution and spread of CO_2 in the water column are very different they all indicate that the footprint of the CO_2 leaked into the ocean will be very constrained to the local vicinity of the leak. Not surprisingly, overall the flux of CO_2 governs the resulting maximum concentration as well as the spatial extent of the dissolved CO_2 plume. Here, the type of leakage, i.e. many leaks dispersed over a large area versus single release point with high flux, is the most important factor. Hence, proper and reliable predictions of the CO_2 migration through the overburden to the seabed are important in order to assess the spatial and temporal footprint in the water column.

Local stratification and current conditions have little influence on the vertical movement and dissolution of gas bubbles, but, once dissolved into the seawater further transport and dilution of the aqueous CO_2 content is highly dependent on local stratification and current conditions, including small scale turbulent mixing. Strong currents will bring the CO_2 cloud over a larger distance in less time, on the other hand strong currents usually implies higher shear, at least along the seafloor, and hence stronger turbulent mixing and rapid dilution. The varying current direction also determines the bearing taken by the CO_2 cloud.

The marine environment is not stagnant and varies due to tides, seasons and storm surges. Proper statistics and understanding of the local conditions will lay the foundation for predicting how the CO_2 signal can be distinguished from natural CO_2 content. Natural variability in, and possible general acidification of, the oceans CO_2 concentration will govern our ability to detect any changes and the potential extra stress imposed on the environment. As long as the signal stays below natural

variability it will be extremely hard to detect, localize and quantify a leak, however, the impact will also be negligible in this case.

The small spatial footprint expected from a CO_2 seep should indicate very localized potential environmental impacts. On the other hand it will make detecting and localizing a leak a bigger challenge.

3. Leakage into atmosphere

Since the emitted CO_2 bubbles are predicted to dissolve within the bottom 5 m above the seafloor, there will be no direct gas flow pathway to the atmosphere. As a consequence direct monitoring of atmospheric CO_2 concentrations is unlikely to be of any utility. Other work (e.g. Blackford et al., 2008; Phelps et al., in press) suggests that most of the emitted CO_2 will eventually outgas to the atmosphere via equilibration of the atmospheric and seawater partial pressures of CO_2. However due to strong hydrodynamic mixing this process will occur over a very wide area, at distance from the source and over periods of some months.

4. Ecological impact

4.1 Methodology

Leakage events, should they occur, could potentially take many forms, depending on CO_2 flux, duration, bubble / jet plume characteristics and the mixing potential of the surrounding water column (Dewar et al., 2013; Blackford et al., 2008). However all leak events will produce a gradient of pH and other chemical change between the leak location and the periphery of the affected area. The length scale of the gradient will depend on leakage characteristics and will likely be dynamic due to tidal mixing. The tractable and generic approach to impact assessment presented here investigates exposure at fixed points along the gradient of pH change from a point where mortality is overriding and rapid (a pH decrease of around 2.0 units, typical of the very epicenter of an emission event) to background or normal pH. The duration of exposure is also critical, short-term exposure, even to large pH perturbations may be relatively inconsequential, whilst long term exposure to moderate perturbations could have a far larger impact on physiology and reproductive success.

For computational practicality a coupled 1-D water column model GOTM-ERSEM (Fig. 10, e.g. Allen and Clarke, 2007) was implemented to study the impact of low pH on zoobenthic communities. These are thought to be the most vulnerable to leakage as they have limited mobility and relatively slow generation times. Pelagic dwelling communities may be impacted, however impacts to fish species will be limited by the ability to escape or avoid temporally deleterious conditions and impacts to plankton will be limited due to rapid advection of replacement populations and fast generation times. The model is detailed in Appendix 3.

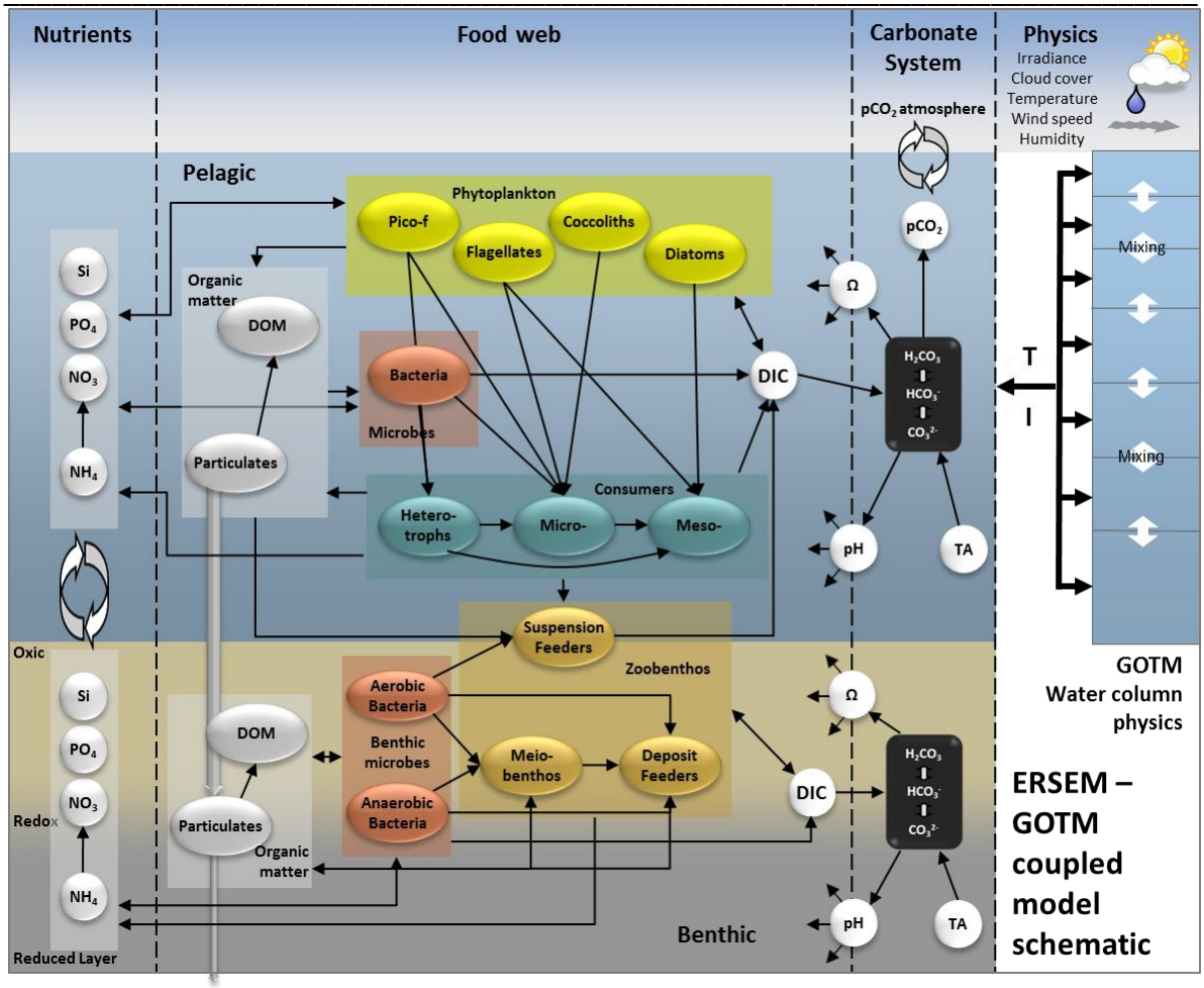

Fig 10. Schematic of the ERSEM-GOTM model system.

Based on literature (as cited in Appendix 3) and expert opinions, model zoobenthic functional groups of suspension-feeders and deposit-feeders were divided into subgroups, classed as either sensitive or tolerant to low pH conditions. These are differentiated by impact thresholds (defined here as a 5% decrease in metabolic activity) at pH = 7.2 and 6.7, respectively (Fig. 11). The impact of pH on the faunal metabolism was parameterised using a hyperbolic function (Fig. 11) applied to the feeding activity rate and the activity respiration rate. Furthermore we implemented an acute response to very low pH adding an extra mortality term when pH is lower than 6. This suite of impacts represents a first-order response of benthic fauna to low pH, which can be summarized in 3 stages:

1. Metabolic depression: the metabolic activity and therefore growth start to decrease. This occurs starting from ~pH<7.2 for the sensitive groups or pH<6.7 for the tolerant groups.
2. Quiescent phase: fauna stops any activity except the basal metabolism. Sensitive fauna enters this stage at pH=6.8; tolerant at pH=6.3.
3. Mortality phase: pH becomes directly toxic for fauna (pH<6.0).

We assumed that meiobenthos does not experience the first two phases because it is adapted to live in an environment with highly variable pH, while filter feeders and suspended feeders experience a relatively more stable pH (being either the in-burrows pH or pelagic pH). Meiobenthos experiences acute mortality at pH <6.0.

Deriving from the average position in the sediment, it was considered that deposit-feeders and meiobenthos respond to benthic pH, while suspension-feeders respond to a combination of benthic and pelagic pH, due to the diverse nature of their feeding strategies

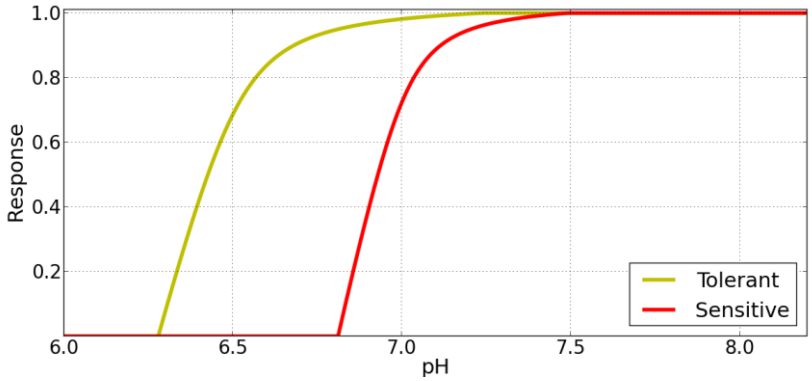

Figure 11. Tolerant (yellow line) and sensitive (red line) responses to lowered pH, applied to uptake rates and activity respiration of zoobenthic groups.

A seep or leak of CO_2 from geological storage will produce two types of impact zone. Within the area of leakage, CO_2 will enter the marine bio-system from below, via the sediments and the first to be exposed will be the deeper sediment dwelling fauna. Away from the area of leakage, impacts will be mediated via mobile plumes of CO_2 rich water permeating the water column. In this case the sediment surface dwelling fauna will be impacted first. Consequently two series of 20-year model runs were conducted: one increasing the flux of dissolved inorganic carbon (DIC) to the sediments and the other adding a DIC flux to the bottom layer of the water column, simulating CO_2 permeating through sediments (at the epicentre of a leak) and an advected CO_2 plume, away from the epicentre, respectively. Each series consisted of 70-100 simulations with progressively increasing additional DIC to replicate a range of delta pH values from 0 to -2.0 pH units. In both cases simulations were conducted until reaching pH values lower than 6.0, i.e. passing the threshold where zoobenthos becomes extinct due to rapid mortality. pH is not held constant during each simulation, but varies according to the normal biological processes that produce seasonality in pH. At the beginning of each model simulation, organisms exerting tolerant and sensitive response to low pH are presumed to be present in equal proportion.

4.2 Results

Results (Fig. 12) are presented as the % change in biomass from a “normal” unperturbed simulation. Results are presented for tolerant and sensitive deposit feeders, tolerant and sensitive suspension feeders and meiobenthos, which are a food source for deposit feeders and resource competitor for both groups and for both the sediment and water column DIC additions.

In simulations where the change of pH is less than ~0.5 units no significant impact is seen. This follows from the parameterisation of the onset of response. For moderate decreases of pH, where an impact is apparent the tolerant groups show an increase in biomass, whilst the sensitive groups show a decrease in biomass. This differential response is ecological in basis. Even though the tolerant groups suffer some reduction in uptake and reduced efficiency, they benefit from the resources released from the more impacted sensitive groups. The response of meiobenthos is similarly ecological, as they benefit from both increased food availability and a decrease in predation during the main growing seasons. At thresholds of change exceeding 1.0 pH units the long term impact of the reduced uptake and efficiency is a decrease in biomass for all functional groups such that after 1-3 growing seasons the biomass loos for the macrofauna is near complete. In these circumstances meiobenthos benefit from the absence of competition and predation and become the dominant faunal class, until mortality kicks in at very large decreases of pH. There is little significant difference between the sediment and water column scenarios – with a long term perturbation DIC equilibrates across the pelagic benthic interface and causes similar changes in pH in both systems. The small differences illustrated are emergent properties of the ecological relationships within the model, where small changes in environmental conditions are frequently amplified by ecological responses. This is not to say that the impact at the epicenter of a leak would be similar to the impact adjacent to the leak, the change in pH at the epicenter is always likely to be significantly larger than the change downstream.

Figure 13 represents a summary of impact category across the pH – time space. Whilst the form of the diagram is likely to be robust, the precise positioning of each category with respect to pH is not definitive and in any case would vary for different ecosystems with different resource bases and faunal components.

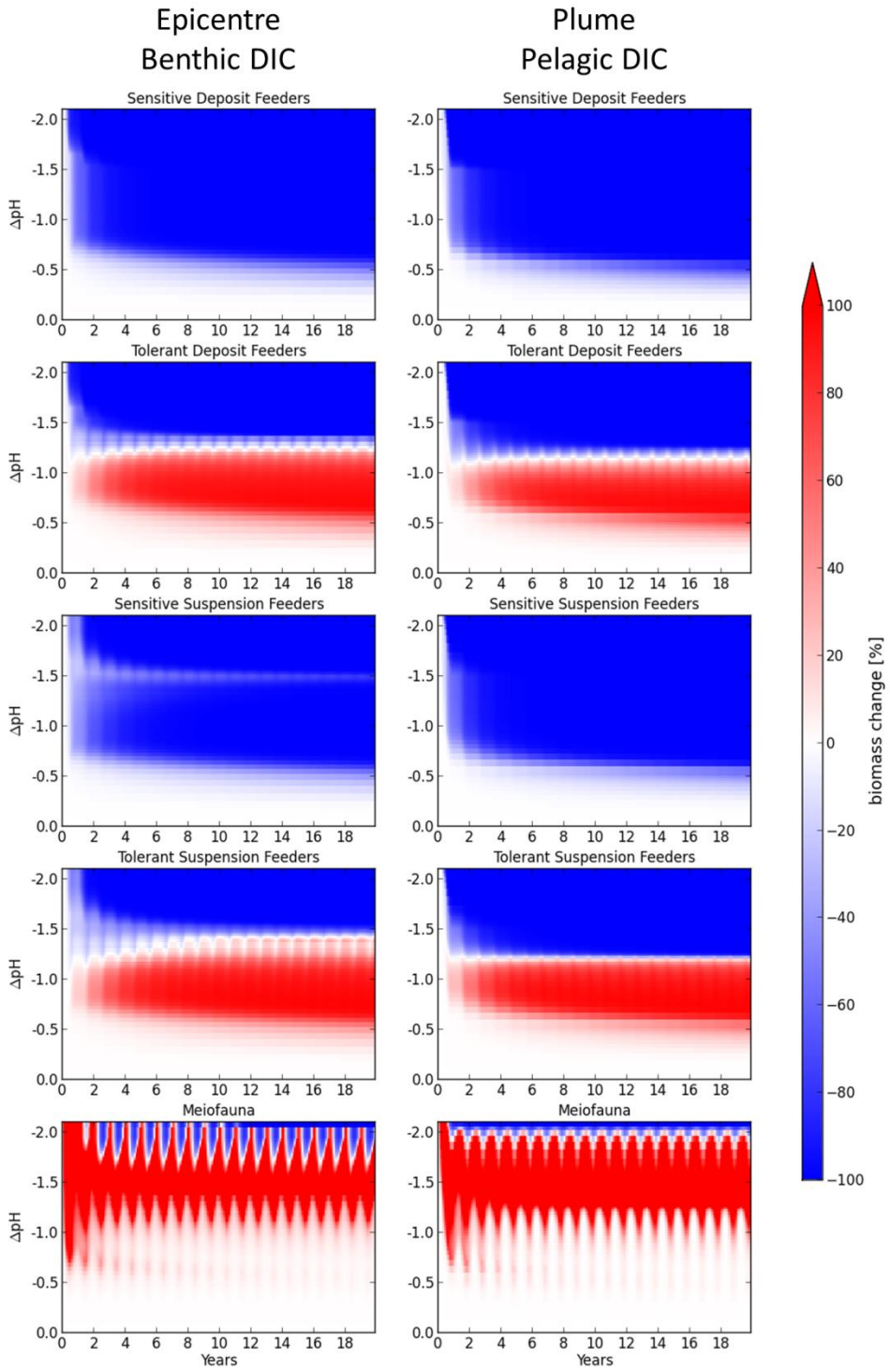

Figure 12: Results of simulation experiment, showing left the epicenter simulations with DIC injected into the sediment layer and right the adjacent plume simulations with DIC injected into the water column. The y-axis represents the mean benthic pH across the run duration. Results show the % change in functional group biomass for, from top to bottom, sensitive deposit feeders, tolerant deposit feeders, sensitive suspension feeders, tolerant suspension feeders and meiobenthos.

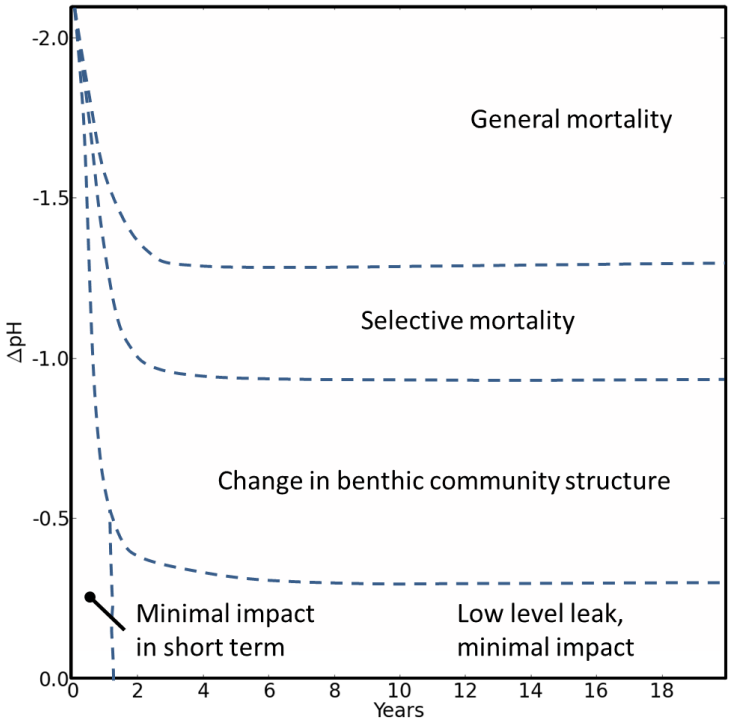

Figure 13: A summary of impact categories across the continuum of pH changes for the first 20 years of a leakage event. The structure of the impact categories is likely to be robust, however the positioning of the boundaries would vary depending on community type and resourcing level.

5. Economic impacts

5.1 Economic project risk assessment

Storage of CO_2 in sub-seabed formations involves a number of uncertainties which can influence the profitability of CCS activities. The profitability, apart from the cost of capturing and transporting CO_2, depends on the one hand on the investment and operational cost of a storage site and, on the other hand, on the return received for storing the CO_2. This return is likely to be a reward that depends on the carbon price that prevails in some climate policy framework. For example, in an emission trading scheme, the operator of a storage facility could get a return for storing CO_2 equivalent to the market price for emissions by avoiding the emission into the atmosphere.

Both the cost of operating a storage facility and the return on storing CO_2 face different types of economic risks. First of all, there is uncertainty about the cost of investment for setting up a safe storage site. Further, there is uncertainty about the potential damage if the storage facility is not as safe as planned. If leakage of CO_2 will occur, it will impact the operation itself as it is likely to be closed at least temporarily and it will impact the income from storing CO_2. Although leakage of significant amounts of CO_2 into seawater and atmosphere is unlikely, see above, we also take into account these small but non-zero probabilities. For the CO_2 becoming

dissolved in the water column in a leakage event, the ecologic damage is reported to be very local and small (see above). We do not consider these costs in the analysis.

Another important uncertainty for the economic viability of CCS concerns the return for storing CO_2. As the price of carbon that can be achieved in the future is uncertain thus affecting the profitability of investing in and running a storage site the investment decision depends on the expected evolution of carbon prices over the time horizon in which a potential storage site can be used.

We use a conceptual model for deriving the option value of investing in a CO_2 storage facility. In a numerical simulation of the option value and the influence of the different types of uncertainty we rely on approximate cost and price estimates. The following economic data were used for the results shown below:

Parameter	Level	Unit
Initial Investment	1,700	Million US$
Operational cost	20	Million US$/year
Resulting Storage Cost	75	US$/t CO_2
Growth rate of carbon price	2	% per year
Volatility of carbon price	0.1	
Leakage hazard rate	1	% per year
Volatility of investment cost	0.05	
Reduction in investment cost	2	% per year

Table 2. Parameter values for the numerical simulation of the option value of investment in sub-seabed storage of 2 Mt/yr over 20 years

This generic storage facility could operate at 75 US$ per ton of CO_2. Because of the uncertainties concerning investment costs, carbon prices, and leakage hazards, but also because of the limited storage capacity of the site an investor would need a carbon price of slightly above 140 US$/t to start investing. At lower carbon prices the discounted profit of starting the operation is lower than the expected profit if the investment is delayed for some time.

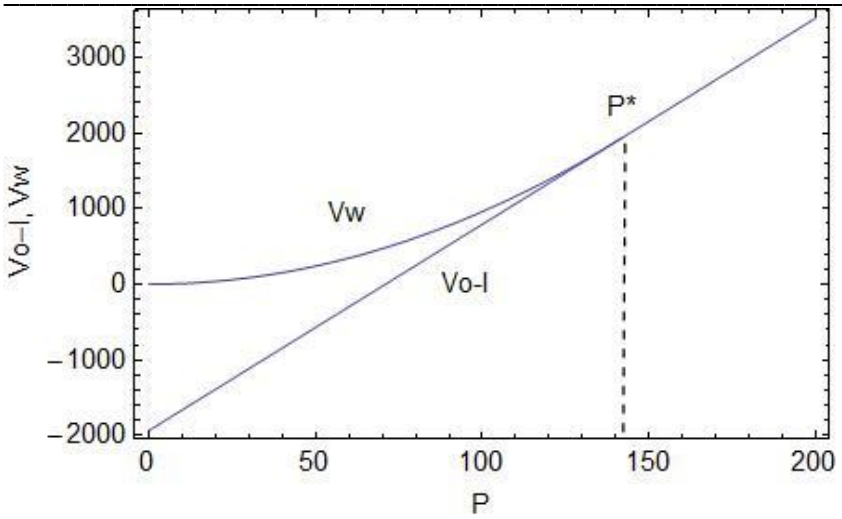

Figure 14: Net present value of CCS operation minus the investment cost (V_0-I) and value of waiting (Vw) as functions of the carbon price.

The uncertainty about the carbon price is the major factor influencing the profitability and the timing of the investment. Figure 15 illustrates the effect of different amounts of uncertainty about the future development of carbon prices, given that on average the carbon price rises at 2 percent per year. With a low volatility of 0.05 the threshold carbon price that triggers the investment would be 125 US$, with a high stochasticity of 0.2 it would be 190 US$. At the assumed growth rate of the carbon price the high uncertainty about future carbon prices would delay investment by over 20 years.

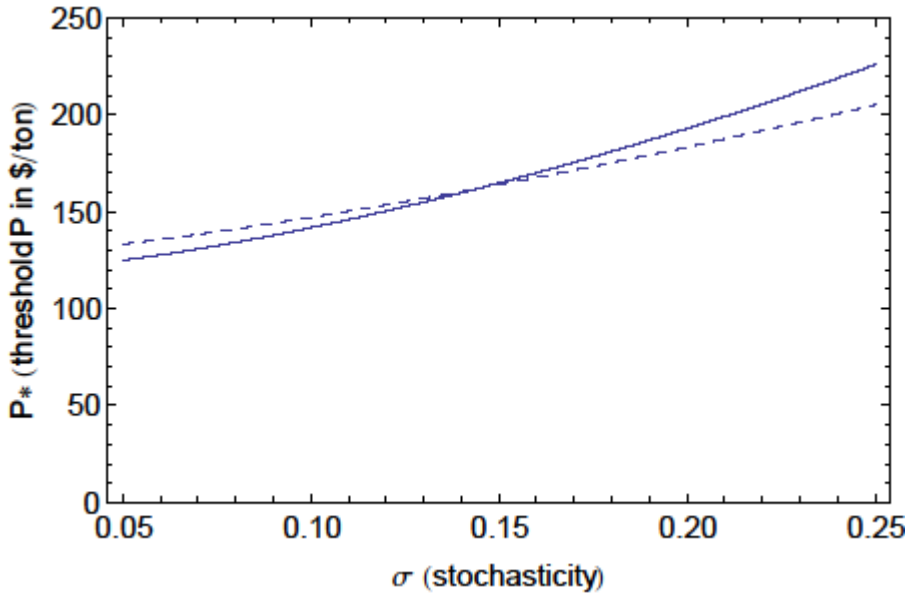

Figure 15: Effect of uncertainty of carbon prices (σ) on the threshold carbon price P*.

The influence of the leakage hazard rate on the timing and the profitability of CCS is very small. At a leakage hazard rate of 1 percent the necessary carbon price would

be 142 US$, if there is no leakage risk, i.e. the hazard rate is zero, the carbon price would be 130 US$ (see Figure 16). The existence of potential leakage would delay investment by only 4 years. Different discount rates (solid line 5 percent, dashed line 10 percent) also do not influence the timing of the investment decision strongly.

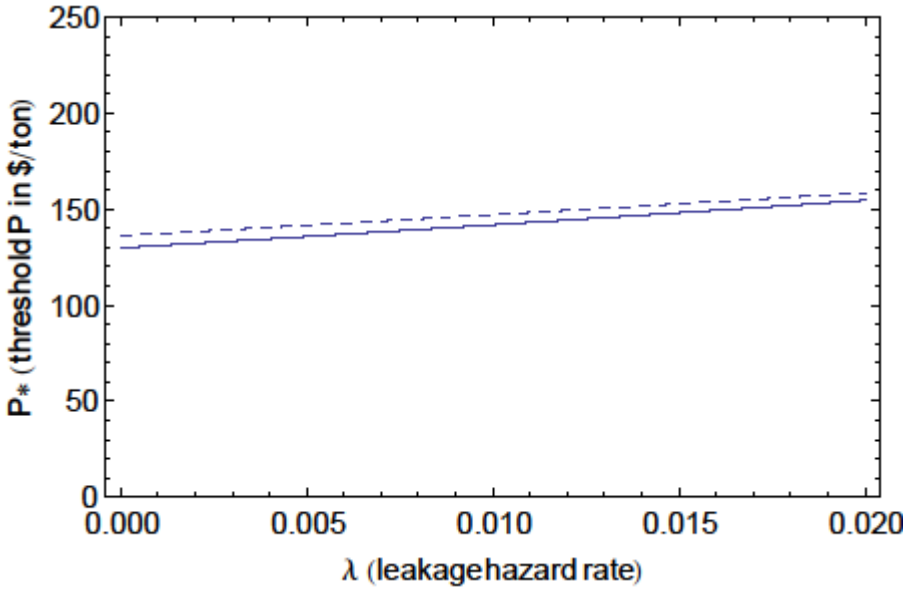

Figure 16: Effect of uncertainty of carbon prices (σ) on the threshold carbon price P*.

In summary: The influence of uncertainty about leakage, investment costs, and income which can be generated through storing CO_2 on the profitability of CCS differs substantially. The numerical model shows that the investment decision to start a sub-seabed storage facility under the above mentioned uncertainties requires a high premium on prices for storing CO_2 for the investor before the present value of the investment is sufficiently large. Since carbon prices are expected to rise over time and investment costs are expected to fall, both with uncertainty about the exact amounts, there is always an incentive to delay investment in CCS until higher carbon prices and lower investment costs promise higher profits.

The risk of leakage is one of the factors determining the timing and profitability of CCS investments but it has the least influence. The profitability is most strongly influenced by the uncertainty about future carbon prices. The larger the uncertainty about the future development in carbon prices, the higher will they need to be in order to trigger investment in CCS. In addition, this means that the commercial decision to implement CCS would be delayed substantially until carbon prices are sufficiently high to compensate for the uncertain returns on investment.

The fact that significant leakage is unlikely does not change the incentives for CCS investments by much. Even though the storage of CO_2 would in this numerical simulation only cost about 75 US$/t CO_2 the required carbon price would be around 130 US$/t CO_2 even without any leakage risk. An unrealistically high leakage risk

would increase the carbon price at which CCS becomes profitable only to 142 US$/t CO_2.

The analysis indicates that the uncertainty concerning the framework conditions for private investment in sub-seabed storage by far dominates any uncertainty about potential leakage. The economic incentives for investing in a sub-seabed storage facility are requiring very high carbon prices in order to compensate for the uncertainty in returns on the storage services provided. A fixed rate of return, e.g. through a guaranteed carbon price for every ton of CO_2 stored could drastically lower the barriers to investment.

5.2 Offshore CCS and Ocean Acidification: A Global Long-Term Probabilistic Cost-Benefit Analysis of Climate Change Mitigation

Public fear for environmental and health impacts or potential leakage of CO_2 from geological reservoirs is among the reasons why over the past decade CCS has not yet been deployed on a large enough scale so as to meaningfully contribute to mitigate climate change. Storage of CO_2 under the seabed moves this climate mitigation option away from inhabited areas and could thereby take away some of the opposition towards this technology. Recent geological studies confirm that leakage for individual offshore CCS operations may be highly unlikely from a technical point of view, if storage sites are well chosen, well managed and well monitored. But we argue that on a global long-term scale, for an ensemble of thousands or millions of storage sites, leakage of CO_2 could take place in certain cases and/or countries for e.g. economic, institutional, legal or safety cultural reasons. We investigated what the impact could be in terms of temperature increase and ocean acidification if leakage would nevertheless occur, and addressed the question what the relative roles could be of on- and offshore CCS if mankind desires to divert the atmospheric damages resulting from climate change. For this purpose, we constructed a top-down energy-environment-economy model, with which we performed a probabilistic cost-benefit analysis of climate change mitigation with on- and offshore CCS as specific CO_2 abatement options.

We predict that CCS is massively deployed as a CO_2 abatement option in order to manage global climate change with CO_2 stored both onshore and offshore. In some 50% of the 100 scenarios, we have a substantial level of around 20 $GtCO_2$ of storage per year around the end of the century, both for onshore and offshore CCS. In the majority of scenarios we see already 10 $GtCO_2$ is geologically stored every year by the middle of the century, and for about 10% of the cases even as much as 40 $GtCO_2$ annually by 2100, with an approximately equal balance between onshore and offshore CCS. Hence, under our current set of assumptions, we observe substantial storage activity for both types of CCS, with onshore CCS benefiting from assumed lower deployment costs and lower leakage rate, while offshore CCS profiting from the lesser damage costs we suppose it incurs.

Figure 17a shows that if the minimum value of the costs of the two CCS options is 20€/tCO_2 or lower, some 80% of overall CO_2 abatement takes place through CCS, rather than other options such as renewables. Even at a 50€/tCO_2 minimum CCS cost it is expected that CCS's contribution to total mitigation efforts is still large, on average about 30%, but there is a non-zero probability that it is close to 0% and could be as high as 60%. At CCS costs between 100€/tCO_2 and 150€/tCO_2, the use of CCS is significantly curtailed, but can still amount to a level contributing by approximately 20% to overall climate mitigation. Figure 17b indicates under what cost conditions which of the two CCS types dominates. If the injection of CO_2 offshore is at most 10% more expensive than onshore injection, then there is at least a 50% probability that offshore CCS is the preferable option, accounting for at least 60% of all CCS deployment. For cost differences of 30%, onshore CO_2 storage becomes more attractive, with an over 50% chance that onshore CCS accounts for more than 60% of all CCS. The explanation for the fact that relatively higher offshore CCS costs can be permitted is the lower level of damages incurred to the environment in the case of leakage of CO_2 into the ocean, in comparison to the case in which leakage occurs into the atmosphere.

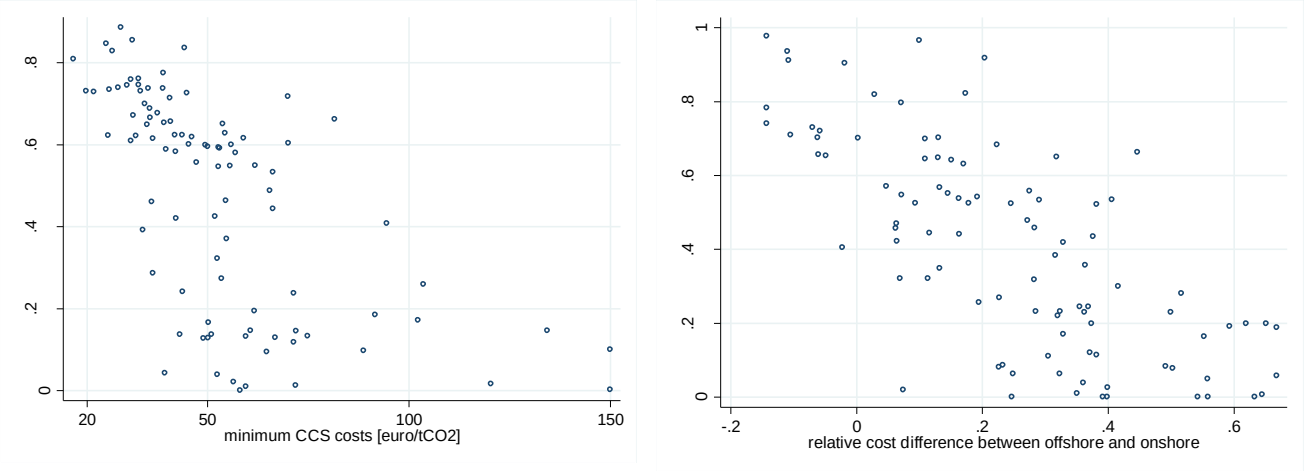

Figure 17: a (left) Share CCS in overall emissions abatement, b (right) Share offshore CCS in total CCS.

The findings reported are different from the conclusions we made in our earlier work on the economics of CCS and leakage of CO_2 (van der Zwaan and Gerlagh, 2009; Gerlagh and van der Zwaan, 2012). We have here attempted to shed light on the possible attractiveness of offshore geological CO_2 storage, and have inspected what the economic benefits could be of complementing onshore CCS with offshore CCS. We find that by allowing for offshore CO_2 storage one could possibly significantly stimulate the usefulness of CCS from a benefit-cost perspective, and thus expand its implementation on such grounds. Offshore CO_2 injection may also substantially reduce public opposition to CCS, which currently plays a sizeable role in impeding its deployment onshore. On the basis of both these perspectives, one may conclude

that partly moving CCS from onshore to offshore may be a beneficial path to take to render CCS practically more feasible and realistic as climate mitigation option.

In short, our argument goes as follows. First, it may well be that CO_2 abatement through offshore CCS is more expensive than via onshore CCS – we assume by around 25€/tCO_2, i.e. 50% in relative terms – given that it is harder to undertake geological CO_2 injection activity under the seabed than directly in open air at the surface of the underground. Second, while not all uncertainty is yet resolved in this domain, it seems very likely that zero-leakage storage sites can be found, operated, maintained and secured (onshore as well as offshore) from a natural scientific point of view. But based on economic, political, institutional and safety cultural arguments one may reason that on a large global scale in which thousands or millions of CO_2 storage sited are being operated, leakage may ultimately not be zero. In such a context, one may claim that offshore leakage is potentially higher than onshore leakage, since the injection process is technologically more requiring and remediation is practically less trivial. We hypothesize that leakage rates could be 50% higher for offshore than for onshore CCS.

One may have different opinions on these two assumptions, and over time they may prove not to hold out. But our main point can be drawn despite these relatively negative hypotheses: even under these conditions, as we demonstrate, offshore CCS may be as interesting from an economic perspective as onshore CCS. As a result, the prospects for CCS could be significantly boosted if one were to shift part of the CCS activities from onshore to offshore territory. The reason for this finding is the assumption that there is high likelihood that the damages from CO_2 leakage directly into the atmosphere onshore, are much more costly than those from seepage into the ocean. Hence, if the circumstances are one day such that a possibility exists for CO_2 leakage, then it becomes much less costly to let the leakage occur into a medium in which the damage costs are relatively modest (whether tangible or intangible) than into one for which these costs are almost certainly high.

In the probabilistic cost-benefit framework that we use for our study, and under the range of stylistic assumptions that we have had to make in order to perform this type of global economic analysis, we find that if offshore storage is at most as costly as onshore storage, then there is a very high probability that at least 60% of all CO_2 capture and storage takes place through offshore CCS. At a 50€/tCO_2 cost of CCS we expect that CCS's contribution to total mitigation efforts is typically about 30%, whereas with CCS costs between 100€/tCO_2 and 150€/tCO_2, the use of CCS is significantly diminished but can still amount to a contribution of around 20% to overall climate mitigation. If the injection of CO_2 offshore is at most 10% more expensive than onshore injection, then offshore CCS is the preferable option, accounting typically for at least 60% of all CCS deployment.

Appendix 1: Detailed information on leakage structures at Sleipner

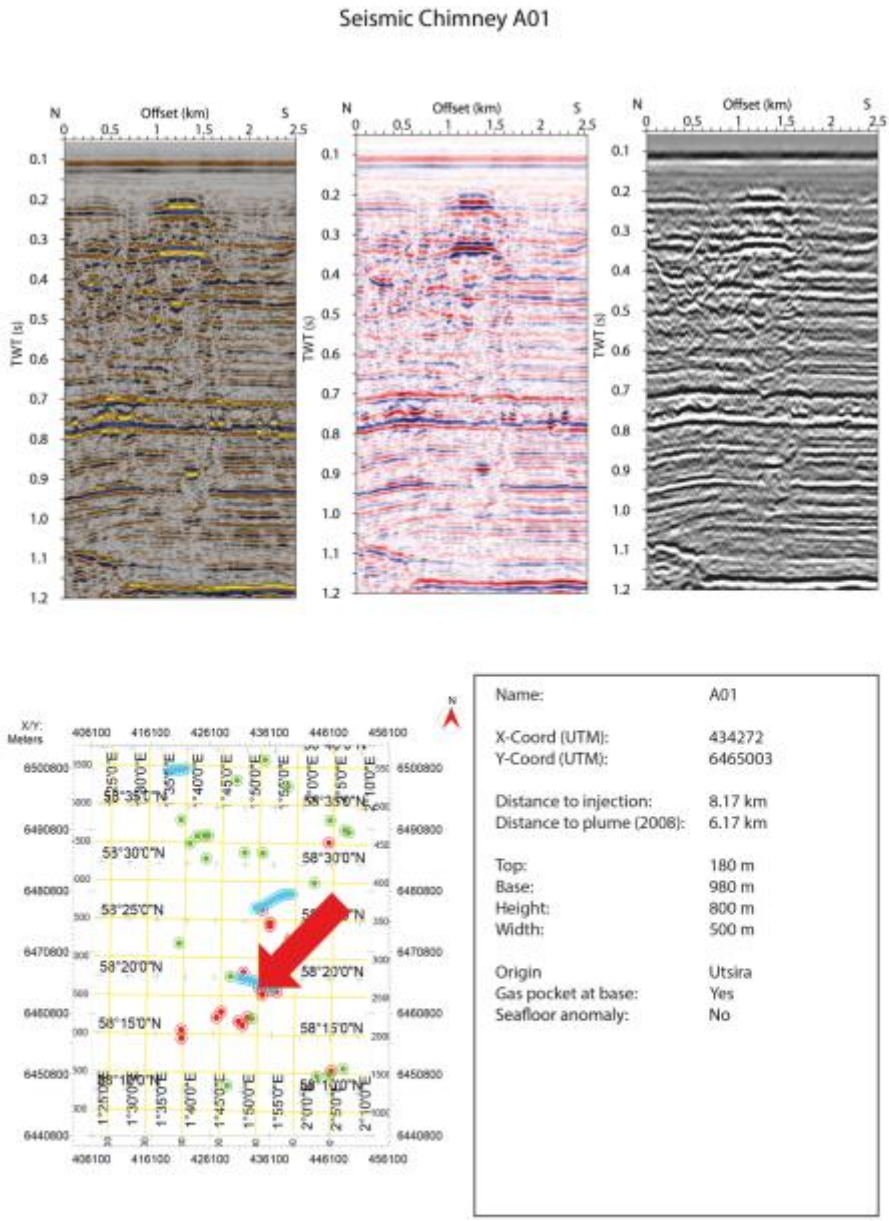

Figure A1.1: Seismic Chimney A01

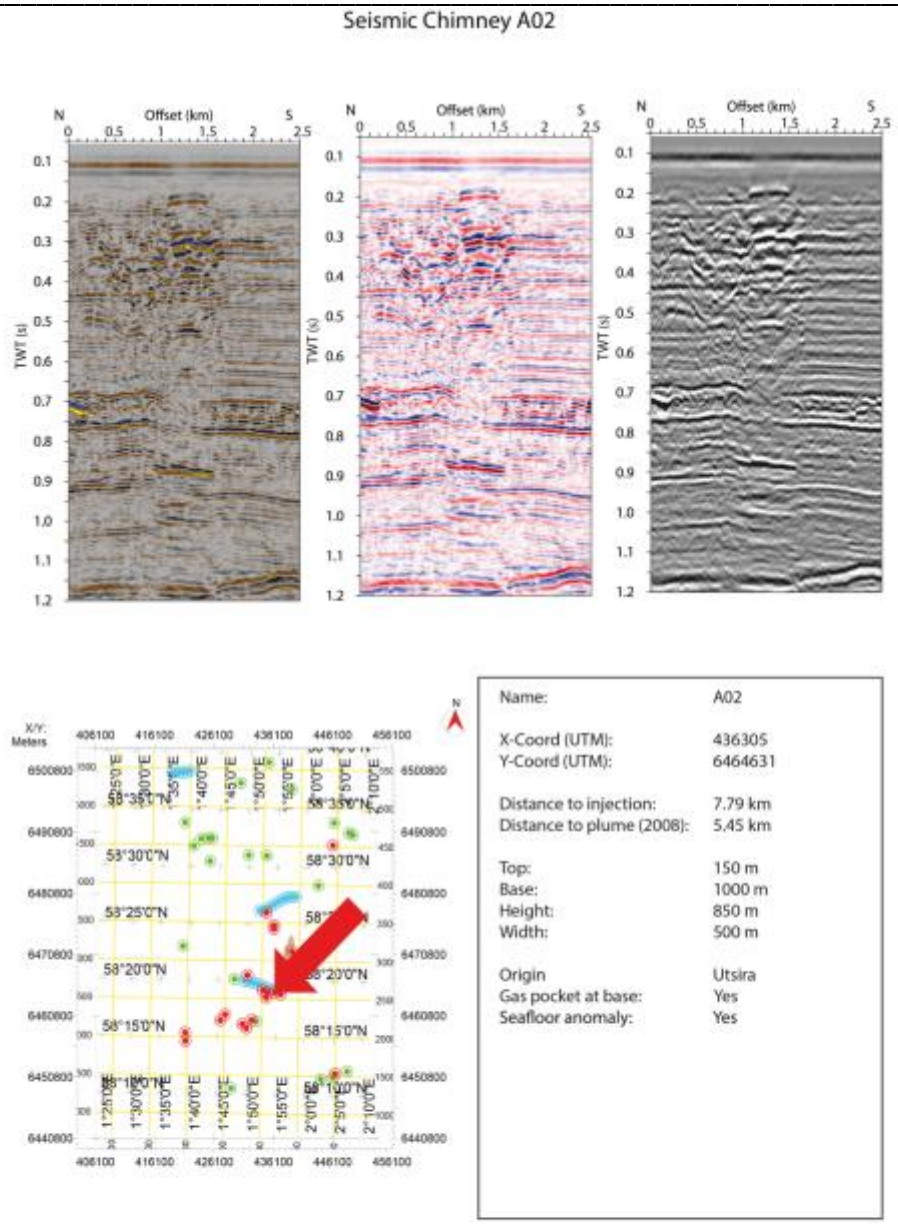

Figure A1.2: Seismic Chimney A02

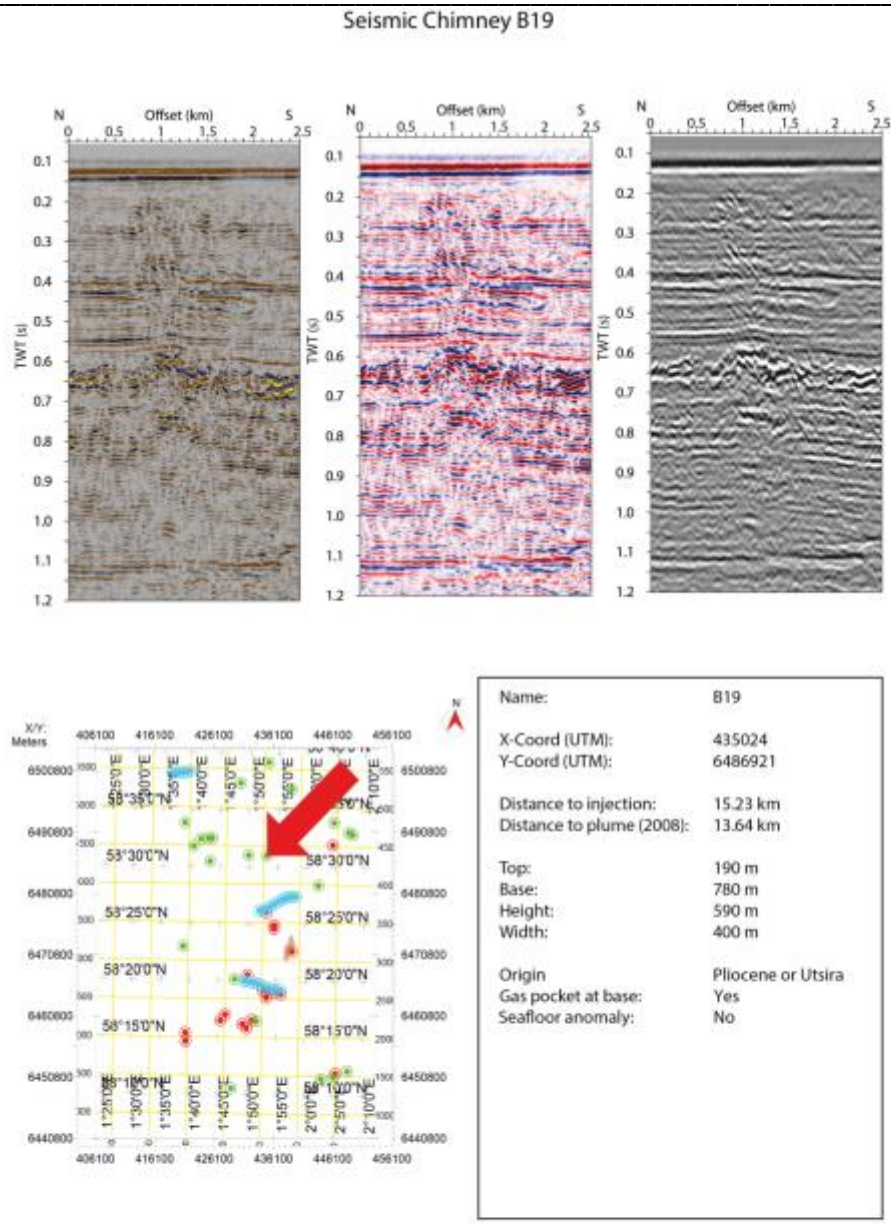

Figure A1.3: Seismic Chimney B19

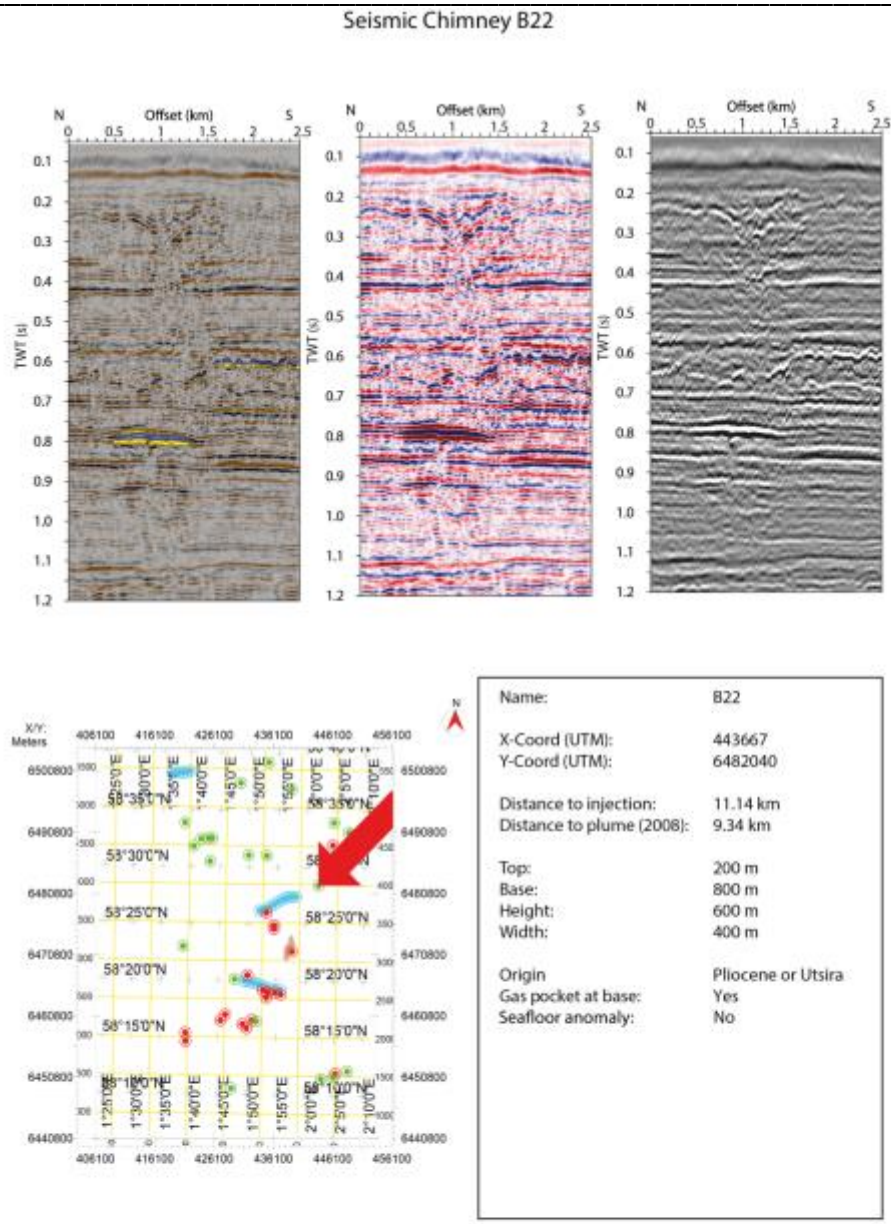

Figure A1.4: Seismic chimney B22

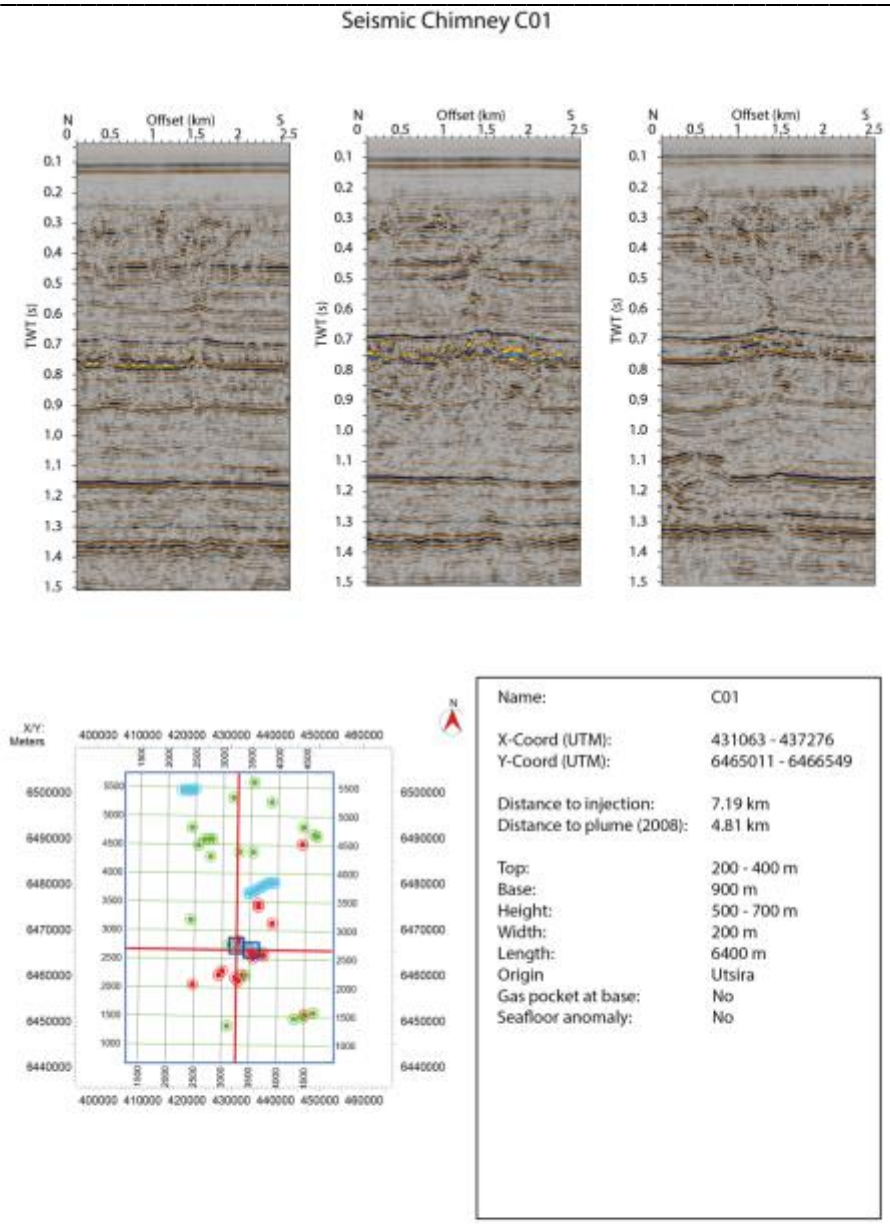

Figure A1.5: Seismic chimney C01

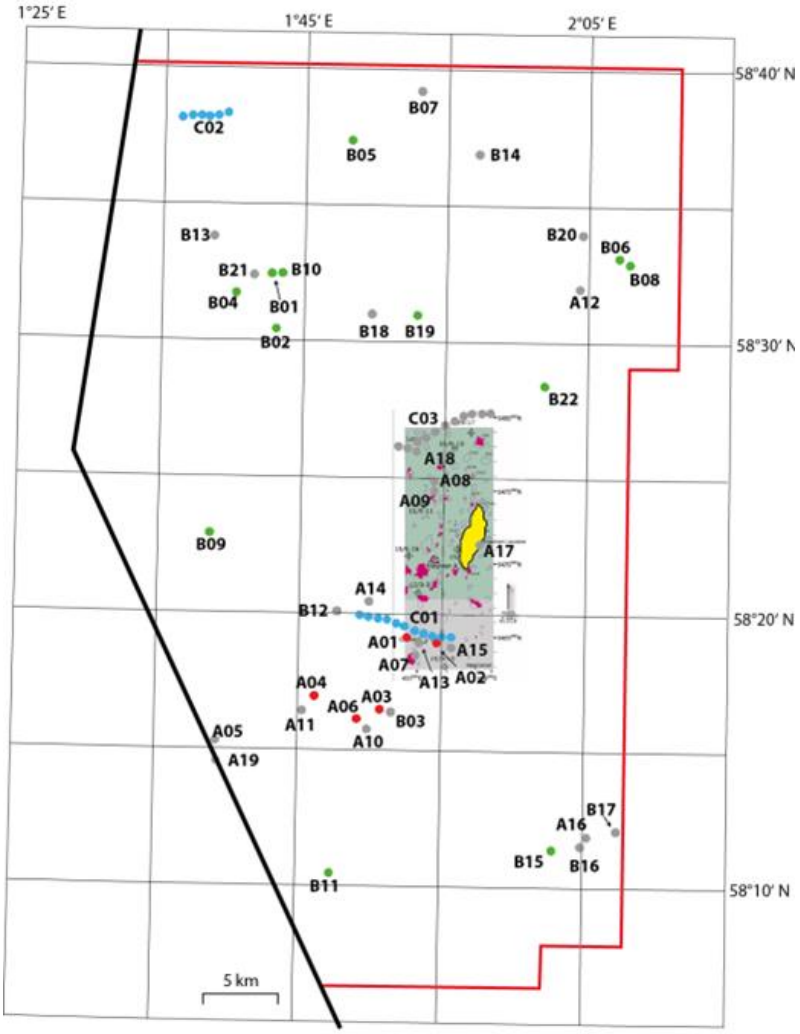

Figure A1.6: Comparison of seismic interpretations of fluid flow structures in the Sleipner area. In his analysis, Nicoll (2011) considered deep pipe structures (labelled as chimney structures) as most relevant for leakage. These features are located beneath strong bright spots at the top of the Pliocene section. However, all of these structures terminate below the top Pliocene and do not show any seismic evidence for continuation to the seafloor. If these features are permeable conduits, CO_2 may migrate along them into the Pliocene section, but will most likely be trapped in this horizon. The large chimney structures identified in Fig. 2, cut through this horizon and therefore are more relevant as leakage pathways.

Appendix 2: Details on leakage simulations through overburden

Sleipner simulations

The Sleipner simulations were conducted in two stages:

(1) 2-phase flow modelling of the spread of the supercritical CO_2 in the Utsira Formation displacing its formation brine for a total simulation time of 200 years considering CO_2-injection at a rate of 1 Mt/yr for 30 years. The model parameterisation was adjusted to match the outlines of the CO_2 plume observed by 4-D seismic data since 1996 (e.g., Arts et al., 2008; Chadwick et al., 2009).

(2) Prediction of possible CO_2 leakage rates and footprints at the seafloor occurring at the identified migration pathways in the larger Sleipner area. 2-phase flow simulations of a total time of 500 years consider the injection of 1Mt/yr of CO_2 for 200 years

Boundary conditions and input parameters:

For all simulations, at the model domain boundaries in the north, south, west and east Dirichlet conditions were applied, whereas the top and bottom were chosen as no-flow Neumann boundaries.

The injection of CO_2 was simulated as a source term in one grid cell within the model domain (Fig. A2.1). In all simulations the same input parameters (Tab. A2.1) were used.

Input Parameter	Value	Reference
Water depth	80 m	
Bottom water temperature	3.4 ^{o}C	Alnes et al. (2011)
Geothermal gradient	31.7 ^{o}C/km	Alnes et al. (2011)
Residual water saturation, S_{wr}	0.11	Singh et al. (2010)
Residual CO_2 saturation, S_{CO2r}	0.21	Singh et al. (2010)
CO_2 injection rate	1 Mt/yr	
CO_2 injection depth	1012 m	Singh et al. (2010)
Capillary entry pressure of Utsira Formation	4 kPa	Chadwick et al. (2012)
Capillary entry pressure of overburden	1.7 MPa	Cavanagh (2013)
Permeability anisotropy of Utsira Formation (K_x : K_y)	0.115 D : 1.15 D	result of plume shape modelling
Permeability of overburden	1e-8 D	

Table A2.1: Input parameters for field scale 2-phase-flow simulations at Sleipner.

Model domains

The simulations of the temporal evolution of the CO_2 plume in the Utsira Formation include only one layer of sedimentary overburden, the upper sand wedge, the thick shale layer below, and the underlying main sand body of the Utsira Formation (Fig. A2.1; for the geology see e.g. Zweigel et al., 2000). In these simulations, none of the potential leakage structures is considered. The CO_2 plume is predicted to reach Well 15/9-13 after about 40 years (Fig. A2.1).

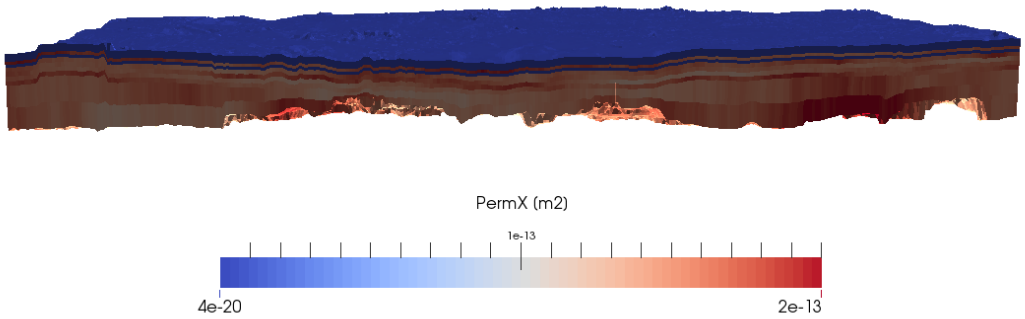

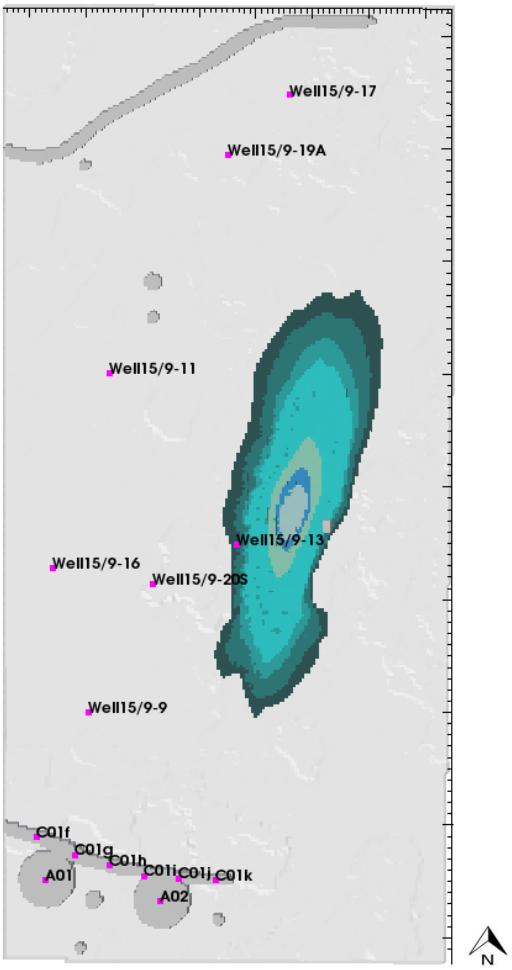

Figure A2.1:

(Top) Model domain of the plume shape simulations with permeability field in X-direction. Model domain is 7 x 20 km^2 and consists of 481293 cells with a grid resolution of 50 m in X- and Y-direction.

(Left) CO_2 plume shape after 6, 9, 13, 30, 50, 100, and 200 years. Note that CO_2 injection is stopped after 30 years in this simulation. The leakage structures are only shown for reference, but are not included in the model.

The model domain of the leakage simulations consequently also included the entire sedimentary overburden and some of the identified leakage structures: A01, A02, and C01 having a direct connection to the Utsira Formation as well as A07, A08, A09, A13, A15, A16, and C03 without a direct connection (Figs. 4 and A2.2). Two different realizations were modelled, one only considering type-A chimneys and the other considering both, type-A and type-C chimneys (Fig. A2.2).

A

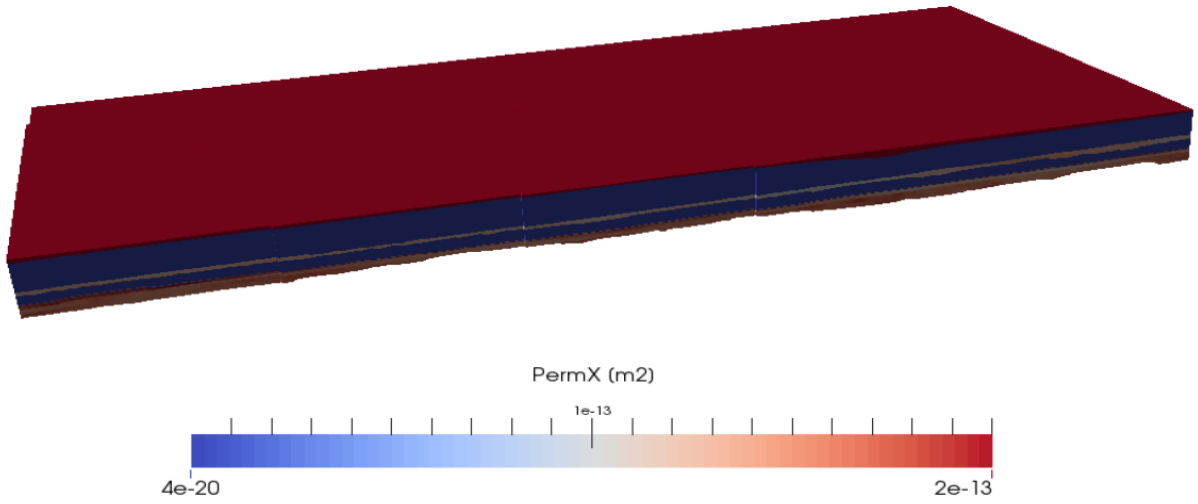

B

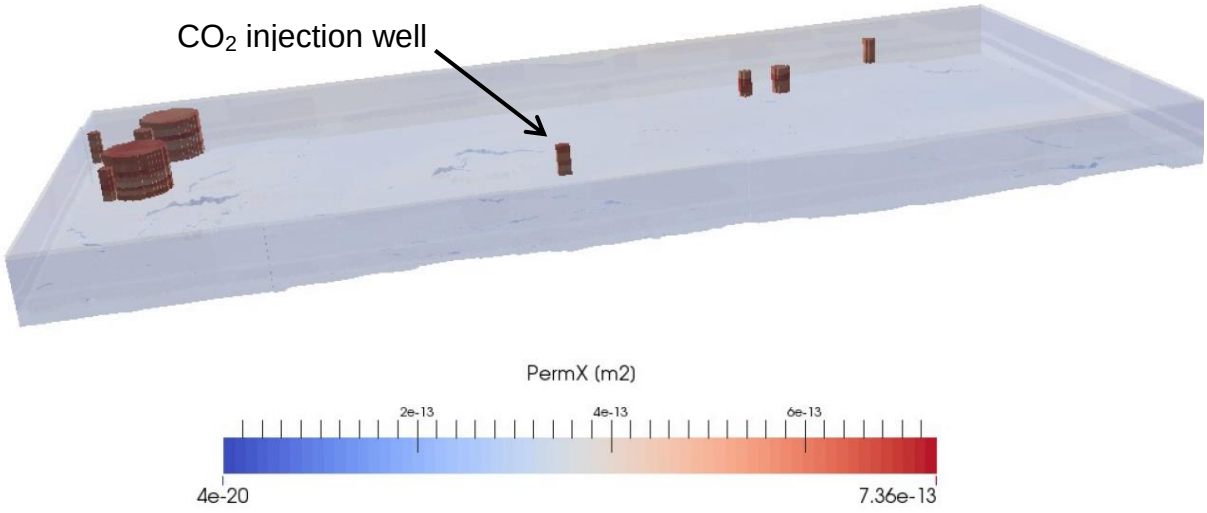

C

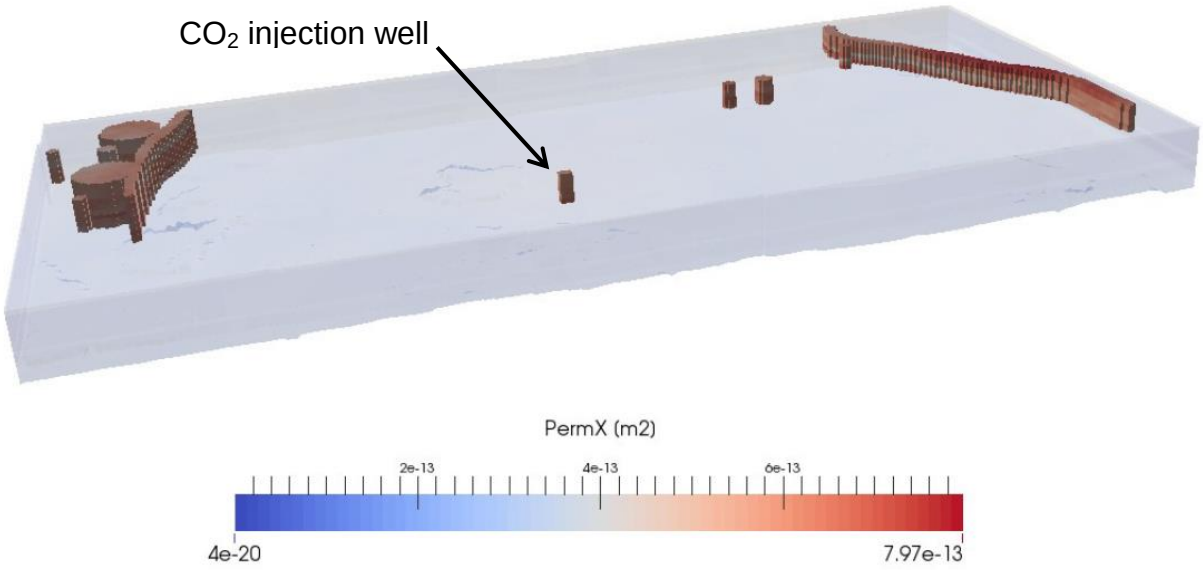

Figure A2.2: (A) Model domain of the leakage simulations with permeability field in X-direction. The model domain is 7 x 20 km^2 and consists of 962586 cells with a grid resolution of 50 m in X- and Y-direction. (B) Model domain showing the permeability distribution in the realization considering only type-A chimneys. (C) Model domain of the realizations considering both, type-A and type-C chimneys and their permeability distribution.

Both leakage realizations, considering only type-A chimneys or also type-C chimneys (Fig. A2.2), predict that the CO_2 will reach the leakage structures in the southern part of the model domain first, calculating leakage at the seafloor to occur either through chimney A02 after 150.2 yr yielding a maximum rate of 108.2 t/d or through chimney C01 after 147.4 yr yielding a maximum rate of 109.8 t/d, respectively (Fig. A2.3). The CO_2 will only flow through a rather small fraction of these large leakage structures producing a footprint at the seafloor of 0.075 km^2 or 0.1 km^2, respectively (red area in Fig. A2.3).

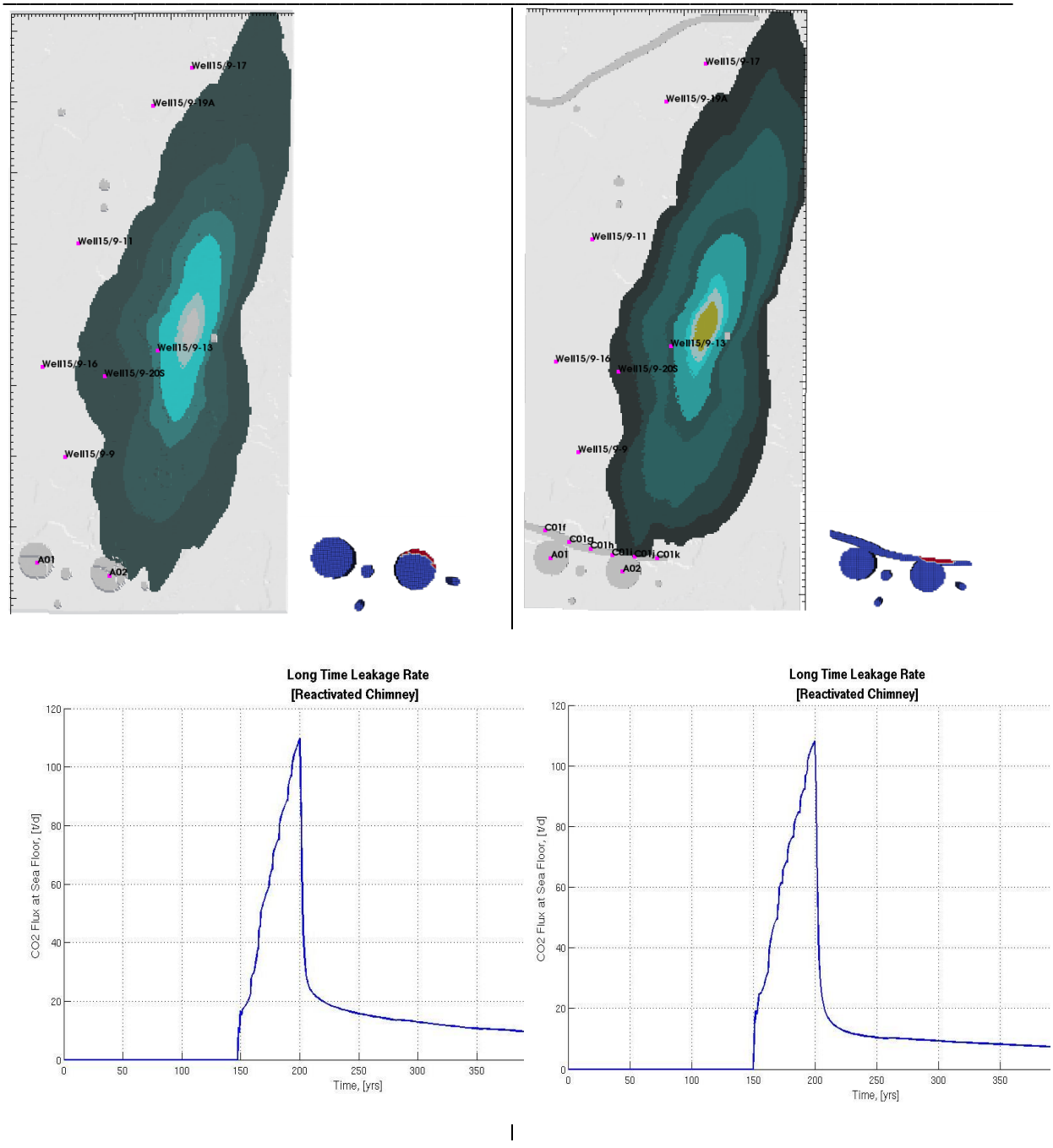

Figure A2.3: CO2 leakage realizations at Sleipner considering (left) only type-A chimneys and (right) type-A & type-C chimneys. (Top) Temporal evolution of the CO_2 plume after 6, 9, 13, 30, 50, 100, 150, and 200 yr (total time of injection is 200 yr) and resulting footprint of the CO_2 leak at the seafloor (red fraction of the blue leakage structure). (Bottom) CO_2 leakage rate at the seafloor over time; the rate drops after injection is stopped in year 200 and slowly fades out over the following centuries.

Snøhvit simulations

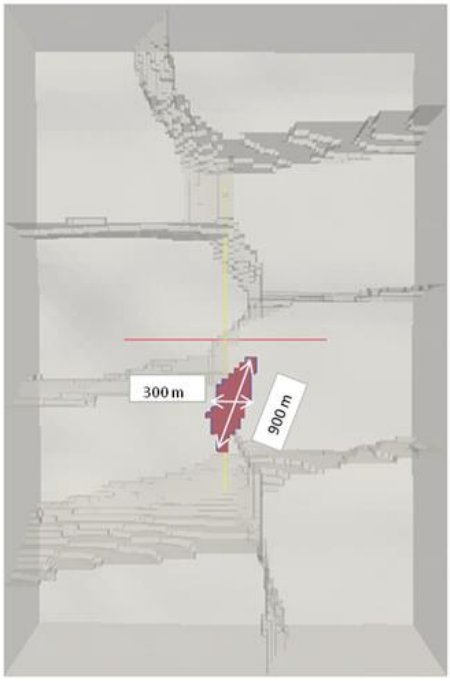

Figure A2.4: Simulated footprint of the seafloor area impacted by CO_2 leakage in the 'Seismic Chimney' scenario (Fig. 5).

Geochemical modelling of the sedimentary overburden

Numerical simulations of the geochemical processes and effects induced by the CO_2 leaking through the sedimentary overburden were conducted with the well-tested diagenetic model C.CANDI (Luff et al., 2001). In this study the focus was on the dissolution of the CO_2 percolating through the leakage structure, the dissolution of reactive minerals in the sediment, particularly $CaCO_3$, and the resulting change in acid-base equilibrium, including pH. Hence, the main porewater/sediment constitutents were total alkalinity (TA), dissolved inorganic carbon (DIC), dissolved Ca, and solid $CaCO_3$. The transient and spatially 1-D simulations are, thus, valid for processes within the leakage pathway and neglect the lateral transport of dissolved CO_2 and other solutes away from the leak. This simplification seems justified because the lateral transport is dominated by diffusion, which is slow. Its time scale can be estimated by the Einstein-Smoluchowski relation:

$$\text{time} = \text{distance}^2 / (2 * \text{diffusion coefficient})$$

e.g., 625 yr for 5 m, 2500 yr for 10 m and so on (assuming a representative diffusion coefficient of 200 cm^2/yr).

Model input parameters for the simulations were based on the environmental conditions at Sleipner (Fig. A2.5). Neumann (no gradient) conditions were used at the upper and lower boundary of the model domain. Since the gaseous/liquid CO_2 phase

itself is not modelled, the geochemical model only estimates the fraction of the CO_2 that gets dissolved and subsequently reacts with carbonates (i.e. is converted into HCO_3^-), or is transported via the aqueous phase into the water column over time. Mass balance calculations are used to estimate the effectivity of the geochemical reactions in mitigating the overall leakage of CO_2.

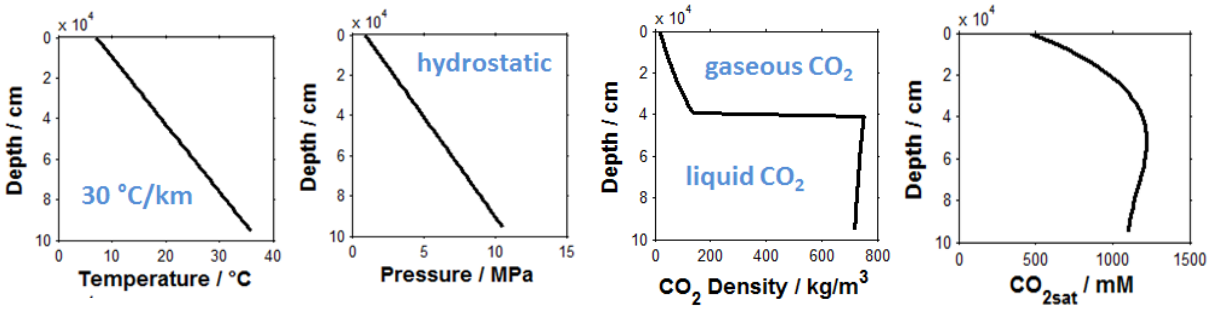

Figure A2.5: Prescribed pressure and temperature conditions as well as resulting density of CO_2 and thermodynamic solubility of CO_2 in the porewater at Sleipner.

Appendix 3: Methodology of ecological impact modelling

ERSEM is a well-tested marine ecosystem model (Blackford et al., 2004) that is configured for temperate shelf seas and includes a benthic food web and biogeochemical model. ERSEM can be coupled to a range of hydrodynamic models in 1D or 3D which code for seasonal forcing and mixing between water masses. In this case the water column General Ocean Turbulence Model (GOTM – Burchard et al., 1999, 2006) is used to represent a one dimensional water column typical of the central North Sea (56N 3E). The model is forced using a climatology of atmospheric data derived from 20 years (1980-2000) of ECMWF-ERA40 reanalysis data (Uppala et al., 2005). In order to properly simulate the onset and the duration of stratification in such a dynamic environment as the North Sea with a simple 1D model, we relaxed the simulated vertical profiles of temperature and salinity to a climatology of the T and S profile simulated by a 3D model of the area running over the same period of time and using the same atmospheric forcing (Holt et al., 2012). The model is run for 5 years with this forcing in order to achieve an equilibrium state that has been used as initial condition for all scenarios. The existing ERSEM model formulation of carbonate chemistry (Artioli et al. 2013), has been recently extended to account for benthic fluxes of alkalinity, thereby enabling the calculation of benthic pH alongside the existing calculation of pelagic pH. A simple formulation of benthic calcification and calcite dissolution was also added. In the model pelagic and benthic pH are driven by concentrations of DIC in the water column and sediment pore water, respectively, thereby defining the end members of the typical benthic profile of pH.

The response of individuals and species to lowering pH is complex. Response can be species specific and highly moderated by habitat trait, nutritional or stress status of the organism (e.g. Thomsen et al., 2013; Pansch et al., 2014). The physiological basis of this response is not yet fully understood and may include aspects of increased metabolic cost, a decrease in uptake, inhibition of reproduction, and mortality (e.g. Dorey et al., 2013). In addition competitive interactions between differently affected predators and prey or competitors for a particular food source are important to consider, as are behavioral responses such as escape. More recently some progress has been made towards a response synthesis (Kroeker et al., 2013) and it is possible to identify classes of animals that are more vulnerable than others; in particular those that depend on carbonate based shells are generally far more sensitive. At the same time it is important to consider the ecological role of species. In this respect the ERSEM model splits the zoobenthos into three functional groups, based on their resource base, either suspension feeders (feeding on particulates at or above the sea floor) and deposit feeders which feed on sedimented material and small organisms within the sediment structure. The latter constitute the third group, called meiobenthos. These functional types also enable a reasonable approach to the physical impacts that zoobenthos have on sediment structure and chemistry, relating to bio-irrigators and bioturbators respectively.

References

Allen, JI; Clarke, KR. 2007Effects of demersal trawling on ecosystem functioning in the North Sea: a modelling study. *Marine Ecology Progress Series*, 336. 63-75. 10.3354/meps336063

Alnes, H., Eiken, O., Nooner, S., Sasagawa, G., Stenvold, T., Zumberge, M. (2011) Results from Sleipner gravity monitoring: updated density and temperature distribution of the CO2 plume. Energy Procedia 4, 5504-5511.

Andresen, K.J. (2012) Fluid flow features in hydrocarbon plumbing systems: What do they tell us about the basin evolution? Marine Geology 332-334, 89-108.

Artioli, Y; Blackford, JC; Butenschon, M; Holt, JT; Wakelin, SL; Thomas, H; Borges, AV; Allen, JI. 2012The carbonate system of the NW European shelf: sensitivity and model validation. *Journal of Marine Systems*, 102-113.

Arts, R., Chadwick, A., Eiken, O., Thibeau, S., Nooner, S. (2008) Ten years' experience of monitoring CO2 injection in the Utsira sand at Sleipner, offshore Norway. First Break 26, 65-72.

Berndt, C. (2005) Focused fluid flow in passive continental margins. Philosophical Transactions of the Royal Society of London A 363, 2855-2871.

Blackford, JC; Jones, N; Proctor, R; Holt, JT. 2008 Regional scale impacts of distinct CO_2 additions in the North Sea. *Marine Pollution Bulletin*, 56. 1461 - 1468.

Blackford, JC; Allen, JI; Gilbert, FJH. 2004 Ecosystem dynamics at six contrasting sites: a generic modelling study. *Journal of Marine Systems*, 52 (1 - 4). 191 - 215.

Burchard, H., K. Bolding, W. Kühn, A. Meister, T. Neumann, and L. Umlauf, Description of a flexible and extendable physical-biogeochemical model system for the water column, *J. Mar. Syst.*, 61, 180-211, **2006**.

Burchard, H., K. Bolding, and M. Villareal. 1999. GOTM - a general ocean turbulence model. Theory, applications and test cases. Technical Report EUR 18745 EN, European Commission.

Cavanagh, A., 2013. Benchmark calibration and prediction of the Sleipner CO2 plume from 2006 to 2012. Energy Procedia 37, 3529-3545.

Chadwick, R.A., Williams, G.A., Williams, J.D.O., Noy, D.J., 2012. Measuring pressure performance of a large saline aquifer during industrial-scale CO2 injection: The Utsira Sand, Norwegian North Sea. International Journal of Greenhouse Gas Control 10, 374-388.

Chadwick, R.A., Noy, D., Arts, R., Eiken, O. (2009) Latest time-lapse seismic data from Sleipner yield new insights into CO2 plume development. Energy Procedia 1, 2103-2110.

Dewar, M., Wei, W., McNeil, D. & Chen, B. Small scale modelling of the physiochemical impacts of CO_2 leaked from sub-seabed reservoirs or pipelines within the North Sea and surrounding waters. *Mar Prod Bull*, 73, 504-515, (2013).

Dorey, N., Lançon, P., Thorndyke, M. and Dupont, S. (2013), Assessing physiological tipping point of sea urchin larvae exposed to a broad range of pH. Global Change Biology, 19: 3355–3367. doi: 10.1111/gcb.12276

Gay, A., Mourgues, R., Berndt, C., Bureau, D., Planke, S., Laurent, D., Gautier, S., Lauer, C., Loggia, D. (2012) Anatomy of a fluid pipe in the Norway Basin: Initiation, propagation and 3D shape. Marine Geology 332-334, 75-88.

Gerlagh, R. and B.C.C. van der Zwaan (2012), "Evaluating Uncertain CO_2 Abatement over the Very Long Term", *Environmental Modeling and Assessment*, 17, 1/2, pp.137-148.

Holt, J., M. Butenschön, S. L. Wakelin, Y. Artioli, and J. I. Allen. 2012. Oceanic controls on the primary production of the northwest European continental shelf: model experiments under recent past conditions and a potential future scenario. Biogeosciences 9:97-117.

Judd, A., Hovland, M. (2007) Seabed Fluid Flow. Cambridge University Press.

Karstens, J., Berndt, C. (revised) Seismic chimneys in the Southern Viking Graben - Implications for palaeo fluid migration and overpressure evolution. Earth and Planetary Science Letters.

Kossel E., Deusner C., Bigalke N., Haeckel M. (2014) Experimental investigation of water permeability in quartz sand as a function of CH4-hydrate saturation. 8th International Conference on Gas Hydrates (ICGH8), Beijing, China, 28 July - 1 August 2014.

Kroeker, K. J., Kordas, R. L., Crim, R., Hendriks, I. E., Ramajo, L., Singh, G. S., Duarte, C. M. and Gattuso, J.-P. (2013), Impacts of ocean acidification on marine organisms: quantifying sensitivities and interaction with warming. Global Change Biology, 19: 1884–1896. doi: 10.1111/gcb.12179

Leifer, I., Judd, A. (submitted) The UK22/4b blowout 20 years on: investigations of continuing methane emissions from sub-seabed to the atmosphere in a North Sea context. Marine and Petroleum Geology.

Linjordet, A., Olsen, R. G. (1992) The Jurassic Snøhvit gas field, Hammerfest Basin, offshore northern Norway. The American Association of Petroleum Geologists.

Luff, R., Haeckel, M., Wallmann, K. (2001) Robust and fast FORTRAN and MATLAB libraries to calculate pH distributions in a non-steady state model for aqueous systems. Computers & Geosciences 27, 157-169.

Nicoll, D. G. (2011) Evaluation of the Nordland Group overburden as an effective seal for the Sleipner CO2 storage site (offshore Norway) using analytical and stochastic modelling techniques. PhD Thesis, School of Geosciences, University of Edinburgh, 383 p.

Nordbotten, J.M., Celia, M.A., Bachu, S., Dahle, H.K., 2005. Semianalytical solution for CO2 leakage through an abandoned well. Environmental Science & Technology 39, 602-611.

Pansch, C., Schaub, I., Havenhand, J. and Wahl, M. (2014), Habitat traits and food availability determine the response of marine invertebrates to ocean acidification. Global Change Biology, 20: 765–777. doi: 10.1111/gcb.12478

Singh, V., Cavanagh, A., Hansen, H., Nazarian, B., Iding, M., Ringrose, P., 2010. Reservoir modeling of CO2 plume behavior calibrated against monitoring data from Sleipner, Norway, Society of Petroleum Engineers Annual Technical Conference and Exhibition. Society of Petroleum Engineers, Florence, Italy, p. 134891.

Thomsen, J., Casties, I., Pansch, C., Körtzinger, A. and Melzner, F. (2013), Food availability outweighs ocean acidification effects in juvenile *Mytilus edulis*: laboratory and field experiments. Global Change Biology, 19: 1017–1027. doi: 10.1111/gcb.12109

Uppala, S. M., KÅllberg, P. W., Simmons, A. J., Andrae, U., Bechtold, V. D. C., Fiorino, M., Gibson, J. K., Haseler, J., Hernandez, A., Kelly, G. A., Li, X., Onogi, K., Saarinen, S., Sokka, N., Allan, R. P., Andersson, E., Arpe, K., Balmaseda, M. A., Beljaars, A. C. M., Berg, L. V. D., Bidlot, J., Bormann, N., Caires, S., Chevallier, F., Dethof, A., Dragosavac, M., Fisher, M., Fuentes, M., Hagemann, S., Hólm, E., Hoskins, B. J., Isaksen, L., Janssen, P. A. E. M., Jenne, R., Mcnally, A. P., Mahfouf, J.-F., Morcrette, J.-J., Rayner, N. A., Saunders, R. W., Simon, P., Sterl, A., Trenberth, K. E., Untch, A., Vasiljevic, D., Viterbo, P. and Woollen, J. (2005), The ERA-40 re-analysis. Q.J.R. Meteorol. Soc., 131: 2961–3012. doi: 10.1256/qj.04.176

van der Zwaan B.C.C., and R. Gerlagh (2009), Economics of Geological CO_2 Storage and Leakage, Climate Change, 93, 3/4, 285-309.

van der Zwaan B.C.C. and K. Smekens (2009), CO_2 Capture and Storage with Leakage in an Energy-Climate Model, Environmental Modeling and Assessment, 14, 135-148.

Vielstädte, L., Karstens, J., Haecke, M., Schmidt, M., Linke, P., Reimann, S., Liebetrau, V., McGinnis, D. F., Wallmann, K. (revised) Quantification of methane emissions at abandoned gas wells in the Central North Sea. Marine and Petroleum Geology.

Zweigel, P., Hamborg, M., Arts, R., Lothe, A.E., Sylta, O., Tommeras, A., Causse, E. (2000) Simulation of migration of injected CO2 in the Sleipner case by means of a secondary migration modelling tool - A contribution to the Saline Aquifer CO2 Storage (SACS) project. SINTEF Petroleum Research, Trondheim.

Zoback, M.D., Gorelick, S. M. (2012) Earthquake triggering and large-scale geologic storage of carbon dioxide. Proceedings of the National Academy of Sciences of the United States of America. 109 (26), 10164-10168.

ECO_2 project number: 265847

Deliverable Number D12.3
Synthesis report on predicted impacts and uncertainties;
WP12/CCT2; lead beneficiary number 2 (PML)

Authors

Report compiled by:
Matthias Haeckel, GEOMAR
Jerry Blackford, PML

With input from:
Alexandros Tasianas, UiT
Jens Karstens, GEOMAR
Waqas Ahmed, U Stuttgart
Marius Dewar, HWU
Lisa Vielstädte, GEOMAR
Guttorm Alendal, UiB
Yuri Artioli, PML
Gennadi Lessin, PML
Gernot Klepper, IfW
Reyer Gerlagh, UVT
Bob van der Zwaan, ECN
Ton Wildenborg, TNO
Bogdan Orlic

18 December 2014